Non-thalamic origin of zebrafish sensory relay nucleus: convergent evolution of visual pathways in amniotes and teleosts

Solal Bloch[1,7#], Hanako Hagio[2,3#], Manon Thomas[1,8], Aurélie Heuzé[1], Jean-Michel Hermel[1], Elodie Lasserre[1], Ingrid Colin[1], Kimiko Saka[4], Pierre Affaticati[6], Arnim Jenett[6], Koichi Kawakami[4,5], Naoyuki Yamamoto[2], Kei Yamamoto[1]*

[1] Paris-Saclay Institute of Neuroscience (Neuro-PSI), Université Paris-Saclay, CNRS, 91190 Gif-sur-Yvette, France

[2] Laboratory of Fish Biology, Graduate School of Bioagricultural Sciences, Nagoya University, Nagoya 464-8601, Japan

[3] Institute for Advanced Research, Nagoya University, Nagoya 464-8601, Japan

[4] Laboratory of Molecular and Developmental Biology, National Institute of Genetics, Mishima, Shizuoka 411-8540, Japan

[5] Department of Genetics, SOKENDAI (The Graduate University for Advanced Studies), Mishima, Shizuoka 411-8540, Japan

[6] TEFOR Paris-Saclay, CNRS UMS2010, INRA UMS1451, Université Paris-Saclay, 91190 Gif-sur-Yvette, France

[7] Present address: Department of Neuroscience, Charleston Alcohol Research Center, Medical University of South Carolina, Charleston, South Carolina 29425, USA

[8] Present address: Plateau de phénotypage TEFOR, LPGP-INRA UR1037, 35042 Rennes, France

[#] These authors equally contributed to the work.

*** CORRESPONDENCE TO:** Kei Yamamoto

Paris-Saclay Institute of Neuroscience (Neuro-PSI), Université Paris-Saclay, CNRS, Avenue de la Terrasse, 91190 Gif-sur-Yvette, France

Tel: +33 1 69 82 42 95

E-mail: kei.yamamoto@cnrs.fr

Running head: convergent evolution of visual pathways

Keywords: sensory ascending; tectofugal visual pathway; thalamus; pallium; forebrain; midbrain; homology; vertebrates; convergent evolution

Abstract

Ascending visual projections similar to the mammalian thalamocortical pathway are found in a wide range of vertebrate species, but their homologous relationship is debated. To get better insights into their evolutionary origin, we examined the developmental origin of a visual relay nucleus in zebrafish (a teleost fish). Similarly to the tectofugal visual thalamic nuclei in amniotes, the lateral part of the preglomerular complex (PG) in teleosts receives tectal information and projects to the pallium. However, our cell lineage study reveals that the majority of PG cells are derived from the midbrain, not from the forebrain. We also demonstrate that the PG projection neurons develop gradually until juvenile stage, unlike the thalamic projection neurons. Our data suggest that teleost PG is not homologous to the amniote thalamus and that thalamocortical-like projections can evolve from a non-forebrain cell population. Thus, sensory pathways in vertebrate brains exhibit a surprising degree of variation.

Introduction

It is accepted that all vertebrate brains possess three major divisions: the forebrain (prosencephalon), midbrain (mesencephalon), and hindbrain (rhombencephalon). The brain morphogenesis established along the anterior-posterior and dorsal-ventral axes of the neural tube occurs at early embryonic states (Figdor and Stern, 1993; Joyner et al., 2000; Echevarría et al., 2003; Stern et al., 2006; Vieira et al., 2010). Neuronal connectivity that determines the brain functions is established at later developmental stages. It is a fundamental question to evaluate to what extent the functional connectivity is conserved among different vertebrate groups (Güntürkün, 2005; Yamamoto and Bloch, 2017; Striedter and Northcutt, 2020).

This issue has been difficult to address, because connectivity patterns are often similar across vertebrate groups. Yet, there is no consensus on the regional homology of the related brain structures across species. This is illustrated by the still ongoing discussions about the evolutionary history of the sensory ascending pathways and thalamorecipient pallial areas in amniotes (a group containing mammals and birds). Notably in birds, different thalamic nuclei convey sensory information to the pallium (Pal; dorsal telencephalon containing the cortex in mammals) in a modality-specific manner. Thus, the avian thalamo-pallial pathway is often compared to the mammalian thalamocortical pathway (Figure 1; amniotes; Th → Pal) (Butler, 1994a, 1994b; Reiner et al., 2005). In contrast, homology of the target pallial areas has been under debate (Karten and Shimizu, 1989; Bruce and Neary, 1995; Striedter, 1997; Puelles et al., 2000; Butler et al., 2011; Dugas-Ford et al., 2012).

One problem is the lack of a sister group representing an intermediate between mammals and birds. Amphibians are the closest outgroup, but unlike amniotes, their sensory projections from the thalamus (Th) mainly terminate in the subpallium (SPa;

ventral telencephalon containing the striatum; Figure 1; amphibians; Th → SPa), with little projections to the pallium (Kicliter, 1979; Neary and Northcutt, 1983; Wilczynski and Northcutt, 1983; Butler, 1994a).

Outside of tetrapods, brain structures are highly divergent compared to amniotes, and thus it is even more complicated to draw an evolutionary scenario. Although teleosts also have sensory afferents to the pallium, the morphology of the teleost pallium is very different from that of tetrapods, as the developmental processes are different (evagination in tetrapods versus eversion in teleosts). Different authors have proposed several hypotheses concerning which part of the teleost pallium would correspond to the mammalian neocortex (Braford, 1995; Wullimann and Mueller, 2004; Northcutt, 2006; Yamamoto et al., 2007; Mueller et al., 2011). Recently, cell lineage studies of the zebrafish pallium have modified the classical view of the eversion model (Dirian et al., 2014; Furlan et al., 2017), and we have proposed a new interpretation on the pallial homology (Yamamoto and Bloch, 2017; Yamamoto et al., 2017).

In teleosts, the controversy is not only on the pallial homology. It has also been debated whether or not the structure giving rise to the major pallial projections is homologous to the tetrapod thalamus (Wullimann and Rink, 2002; Northcutt, 2006; Yamamoto and Ito, 2008; Mueller, 2012). This structure is named the preglomerular complex (PG; Figure 1; teleosts; PG → Pal). In order to determine the evolutionary scenario of sensory pathways in bony vertebrates (Osteichthyes), it is important to investigate whether or not the teleost PG is homologous to the amniote thalamus.

As for the controversy on the pallial homology, different authors claim different hypotheses. On the one hand, based on descriptive embryology, the teleost PG has been considered to originate from the basal portion of the diencephalon, the posterior tuberculum (Bergquist, 1932; Braford and Northcutt, 1983; Butler and Hodos, 2005;

Northcutt, 2008; Vernier and Wullimann, 2009), unlike the thalamus that originate from the alar portion of the diencephalon.

On the other hand, due to the similar connectivity patterns of sensory pathways, it has also been proposed that PG may be homologous to the thalamus (Yamamoto and Ito, 2008; Ito and Yamamoto, 2009). PG receives various sensory inputs of different modalities (e.g. visual, auditory, lateral line, gustatory, and possibly somatosensory), and gives rise to ascending projections to the pallium (Striedter, 1991, 1992; Yoshimoto et al., 1998; Yamamoto and Ito, 2005, 2008; Northcutt, 2006; Ito and Yamamoto, 2009). Notably, the tectofugal visual pathway has been well investigated, and it has been compared to the one in amniotes. In goldfish and carps, the lateral preglomerular nucleus (PGl) receives visual information from the optic tectum (TeO) and projects to the lateral part of the dorsal telencephalic area (Dl) within the pallium (TeO → PG → Pal; Figure 1) (Yamamoto and Ito, 2005, 2008; Northcutt, 2006). This is similar to the tectofugal visual pathway or extrageniculate pathway in mammals: the visual thalamic nucleus (pulvinar in primates, and lateral posterior nucleus in other mammals like rodents) receives inputs from the TeO (superior colliculus -SC- in mammals) and projects to the visual pallium (extrastriate visual cortex in mammals) (SC → Th → Pal; Figure 1). In addition, the relative size and complexity of the PG are correlated with the complexity of the pallial connections, similarly to what has been documented in the tetrapod thalamus (Northcutt, 2008).

Some other studies have suggested PG is composed by migrated cells (Wullimann et al., 1999; Mueller and Wullimann, 2002) and that Pax6-positive (Pax6+) alar diencephalic cells migrate ventrally to form the PG during development (Wullimann and Rink, 2001, 2002; Ishikawa et al., 2007).

More recently, our cell lineage study in zebrafish has shown that many PG cells are indeed migrating from the midbrain region, instead of the diencephalon (which is in the forebrain). The ventral brain regions containing PG, the torus lateralis (TLa), and the inferior lobe (IL), which were considered to be part of the forebrain, are indeed composed of cells migrating from the midbrain-hind boundary (MHB) (Bloch et al., 2019). These data strongly suggest that the PG is not, as a whole, homologous to the amniote thalamus. Bloch et al. (2019) focused on the development of IL, and it is still not clear whether the midbrain-derived cell cluster contains the PG-pallial projection neurons.

Thus, this study aims to clarify the developmental origin of the PG neurons comprising an ascending tectofugal visual pathway. Combining tract-tracing and cell lineage studies, we confirmed that the majority of the PG cells, including the PG-pallial projection neurons, originate from the mesencephalic region. Thus, the teleost PG is not homologous to the amniote thalamus, and their similar connectivity pattern would have evolved independently in each animal group.

Results

Zebrafish transgenic line labeling the visual afferent projection to the pallium

In order to generate a transgenic line that labels the "thalamocortical-like pathway" in zebrafish, we performed a genetic screen using the *Tol2* transposon-based gene trap construct, and collected transgenic fish with expression of the engineered Gal4 transcription factor in specific cell populations. The Gal4 expression was visualized by crossing the transgenic fish with a reporter line carrying EGFP under the control of UAS (*Tg(UAS:GFP)*) (Asakawa and Kawakami, 2009; Kawakami et al., 2010; Lal et al., 2018).

Among these lines, we identified a Gal4-expressing transgenic fish line, *Tg(gSAGFF279A*) crossed with *Tg(UAS: GFP)*, which had GFP-positive (GFP+) cells projecting to a part of the pallium (Supplementary file 1). We analyzed the genomic DNA from the transgenic fish by Southern blot and inverse PCR, and found that the gene trap construct was integrated within an intron of the *inpp5ka* (inositol polyphosphate-5-phosphatase Ka) gene (Supplementary file 2). Hereafter, we simply refer to this double transgenic line *Tg(gSAGFF279A;UAS:GFP)* as *Tg(279A-GFP)*, and always used the offspring screened with GFP expression.

In the *Tg(279A-GFP)*, abundant GFP+ fibers are present in Dl (Figure 2A), and GFP+ cell bodies are found in a part of PG (Figure 2B). 3D reconstruction of confocal images of the entire brain allowed us to follow the projection from the PG to the pallium (Figure 2C,D and Video 1). We confirmed that axonal projections originating from the PG terminate on the ipsilateral Dl (Figure 2C and Video 1).

This projection from PG to Dl is very similar to the ascending visual projection of other cyprinid species such as goldfish and carp (Yamamoto and Ito, 2008). In goldfish and carp, the vast majority of retinal axons terminate in TeO, and TeO neurons project to the lateral preglomerular nucleus (PGl), which in turn projects to the Dl in the pallium. In *Tg(279A-GFP)* zebrafish brain, GFP+ cells form a cluster within a nucleus corresponding to the goldfish PGl. Sagittal sections through the lateral part of PG demonstrate the GFP+ cell cluster as a prominent oval-shaped structure (Supplementary file 1A). Thus, based on the comparison with other cyprinids, we here refer to the GFP+ PG cell cluster projecting to Dl as PGl.

The PGl-Dl projection is not yet observable at 4 weeks post-fertilization (wpf) (Figure 3A, B, Supplementary file 3). A few GFP+ cell bodies appear at the level of PG around 6 wpf. The GFP+ cell cluster in PG (which we consider as PGl) becomes

prominent at 8 wpf (Figure 3D) yet the GFP+ fiber labeling in Dl appear very weak at this stage (Figure 3C). At 3 months post-fertilization (mpf), there are around 200 GFP+ cells in PG in each hemisphere (Figures 2B-D, 3F, Supplementary file 1I), and they have abundant projections to Dl (Figures 2A,C,D, 3E, Supplementary file 1F).

Validation of the tectofugal visual pathway in zebrafish

In order to verify whether the GFP+ projections correspond to the ascending visual pathway in zebrafish, we performed tract tracing studies using DiI, biocytin, or biotinylated dextran amine (BDA).

It has been known that retinal projections terminate in the upper layers of TeO in a wide range of species of ray-finned fish (von Bartheld and Meyer, 1987), and it is also the case in zebrafish (Supplementary file 4). In order to confirm whether the zebrafish PG receives visual inputs from TeO, we injected DiI in the PG of the *Tg(279A-GFP)* line, targeting the lateral subdivision (PGl) with a guide of GFP (Figure 4A, asterisk). After 2-3 weeks of incubation, we observed retrogradely labeled cell bodies in a deep layer of TeO (Figure 4B). The cell extends its dendrites up to the retino-recipient upper layer of TeO (the stratum fibrosum et griseum superficiale; SFGS), and this morphology is identical to the neurons receiving the retinal input in carp and goldfish (Yamamoto and Ito, 2008). BDA injection into TeO (Figure 4C, asterisk) labeled axon terminals in the PGl (Figure 4D, arrowheads), confirming that PGl receives tectal inputs.

Following the biocytin injection in PGl (Figure 4G, asterisk), we observed abundant fiber labeling in Dl (Figure 4H). This Dl labeling pattern is identical to the GFP+ fiber labeling of the *Tg(279A-GFP)* (Figures 2A and 4I). Conversely biocytin injection into Dl (Figure 4J, asterisk) labeled perikarya of PGl neurons (Figure 4K),

coinciding with the position of the GFP+ cells in *Tg(279A-GFP)* (Figure 4L, arrowheads). These data confirm that PGl neurons project to Dl of the pallium.

Thus, we conclude that the PGl conveys visual information from TeO to Dl, and that the GFP+ projection from PGl to Dl in *Tg(279A-GFP)* recapitulates this visual pathway.

Mesencephalic progenitors give rise to the GFP+ PGl cells

Based on a cell lineage method using tamoxifen inducible Cre-lox recombination, we recently revealed that some brain structures that have been considered to be of prosencephalic origin (forebrain) are actually of mesencephalic origin (midbrain) (Bloch et al., 2019). PG was one of them (Figure 5, Supplementary file 5), thus we further investigated the development of PG cells, including those in PGl.

We used a double transgenic line generated by crossing *Tg(her5:ERT2CreERT2)* and *Tg(βactin:lox-stop-lox-hmgb1-mCherry)*, in which mCherry is expressed in the progenies of *her5*-expressing cells by a tamoxifen induction. The transcription factor *her5* is exclusively expressed in the midbrain-hindbrain boundary (MHB) at 24 hours post-fertilization (hpf) (Figure 5A), and in ventricular cell clusters in the midbrain at juvenile stages (Galant et al., 2016; Bloch et al., 2019).

By following the mCherry-positive (mCherry+) cells at different developmental stages after induction at 24 hpf, we observe that PG is constituted as the most rostro-ventral end of a cell cluster migrating from the MHB (Figure 5B, D, F). The *her5*-mCherry+ cells are distributed in the entire PG, including PGl where the 279A-GFP+ pallial projection neurons are located (Figure 5 and Supplementary file 5). Counting mCherry+ cells from individuals induced at different time points suggests that at least

60% of PG cells originate from the midbrain region (Supplementary file 6). Thus, we conclude that the majority of PG cells, if not all, are of the midbrain origin.

To further confirm whether the GFP+ and mCherry+ signals co-localize, we generated a quadruple transgenic line *Tg(her5:ERT2CreERT2;βactin:lox-stop-lox-hmgb1-mCherry;279A-GFP)* (Supplementary file 7A), and performed tamoxifen induction at 24 hpf. We have verified that the quadruple transgenic line is identical to the double transgenic lines in terms of expressions of GFP and mCherry, and that their brain development is unaltered. Observing the PGl in the adult stage (3 mpf), we found that there are PGl cells co-expressing both GFP and mCherry (Figure 4D-G, arrowheads). This suggests that at least some of the GFP+ pallial projection neurons originate from the MHB.

Since the GFP+ projection neurons become observable after 4 wpf (Figure 3), we hypothesized that they may be generated also during the juvenile stages. Thus, we decided to perform the tamoxifen induction at different developmental stages. However, the fertility of the *her5* quadruple transgenic line (number of eggs and survival rate of young larva) were relatively low. For this reason, we used an additional transgenic line for the induction at later developmental stages.

As an alternative to the *Tg(her5:ERT2CreERT2)*, we used *Tg (Dr830:ERT2CreERT2)* (Heuzé, 2017) (Supplementary file 7B). The enhancer sequence "830" (human enhancer is named "*Hs830*", and zebrafish enhancer is "*Dr830*") is a highly conserved regulatory sequence in mouse and in zebrafish, which acts as a putative enhancer of the transcription factor *Meis2* (*meis2a* in zebrafish) selectively in the tectum (Heuzé, 2017). In this line, the expression territory of Cre is larger than *Tg(her5:ERT2CreERT2)* at 24 hpf, but the expression is limited to the tectal area after 30-48 hpf (Figure 7 and Supplementary file 8). We first generated the double

transgenic line *Tg(Dr830:ERT2CreERT2;βactin:lox-stop-lox-hmgb1-mCherry)*, then crossed with *Tg(279A-GFP)*, in order to generate a quadruple transgenic fish *Tg(Dr830:ERT2CreERT2;βactin:lox-stop-lox-hmgb1-mCherry;279A-GFP)* (Supplementary file 7B).

We performed tamoxifen induction at different developmental stages from 24 hpf up to 8 wpf (Supplementary file 9), and examined the adult brains to verify whether GFP+ pallial projection neurons co-express mCherry. We found GFP/mCherry co-expressing cells consistently in all the induction time-points until 6 wpf (Figure 8). The abundance of mCherry+ cells became less and less along development. At 6 wpf, there were very few mCherry+ cells in PGl, and we found only one cell co-expressing GFP and mCherry among all the specimens examined (Figure 8G). We didn't observe any co-expression in the case of induction at 8 wpf.

Thus, our results suggest that GFP+ PGl cells are gradually added throughout the larval/juvenile stages around up to 6 wpf. Considering the small number of GFP+ cells in PGl and the short-term tamoxifen induction time, it would be reasonable to conclude that majority of GFP+ pallial projection neurons are progenies of cells derived from the tectal region.

Discussion

Ontogeny of the zebrafish PG

By using tamoxifen inducible Cre-lox system in zebrafish, we labeled by mCherry the cells that were located in the midbrain region during development (between 24 hpf and 6 wpf). Abundant mCherry+ cells in the adult PG suggests that majority of PG cells derive from the mesencephalic region. PG cells were consistently labeled with mCherry following the treatments at all the developmental stages examined. This

suggests that PG progressively grows by addition of cells migrating from the mesencephalon.

It is difficult to prove whether all the PG cells originate from the mesencephalon, due to the technical limitation of the tamoxifen induction. Long term tamoxifen treatment leads a high mortality rate of the fish during the experiment (Bloch et al., 2019; Yu et al., 2019). Moreover, the Cre-lox system would not allow 100% induction rate (Hayashi and McMahon, 2002). Thus, mCherry labeling of each experiment represents only a small fraction of the cells originating from the mesencephalic region.

Thanks to the *Tg(279A-GFP)*, we could label visual pallial projection neurons in PG. There are only about 200 GFP+ neurons in the adult PG. In the quadruple transgenic lines expressing both GFP and mCherry, we observed consistently at least one or two co-expressing cells whenever the tamoxifen induction was performed before 6 wpf. Considering the short duration of each tamoxifen treatment, it may be reasonable to assume that most of the GFP+ cells originate from the midbrain. Thus, we conclude that the PGl projection neurons to the pallium are mainly composed of cells migrating from the mesencephalon, by gradual accumulation from embryonic to juvenile stages (until around 6 wpf). The absence of mCherry/GFP colocalization at 8 wpf suggests that the PGl reaches maturation around this stage, as indicated by the abundance of the projections to the Dl (Figure 3C,D).

At early embryonic stages in both quadruple transgenic lines, the Cre expression appears to extend from dorsal to ventral MHB, therefore it is hard to conclude whether the PG cells derive from the alar or basal portion. A recent publication using *shh*-GFP transgenic line suggests that the adult PG contains *shh*-expressing cells (GFP+ in the transgenic line), indicating that some PG cells may be of basal origin (Wullimann and Umeasalugo, 2020). However, the expression of Cre at later stages is limited to the

alar portion of the mesencephalon (notably tectal area). Thus, PG cells are migrating from the alar mesencephalic region at least at juvenile stages. This is consistent with previous studies claiming the PG is comprised of Pax6-expressing migrating cells (Wullimann and Rink, 2001; Ishikawa et al., 2007): both thalamic and tectal regions are Pax6+ domains. The data of the previous studies were interpreted assuming that the PG cells should come from the forebrain, leading the conclusion that the Pax6+ cells should be thalamic or prethalamic. Our data show that the PG cells are mesencephalic, thus they are probably derived from Pax6+ tectal cells.

GFP+ fiber labeling in Dl appears to be prominent only at around 8 wpf (Figure 3C). Unlike the thalamocortical projections in mammals that are already abundant at late embryonic stages, the visual ascending projections to the pallium in zebrafish are not mature until late juvenile stages. Yet zebrafish larvae can coordinate body orientation against the current, capture food, or escape from predators using relatively simple tectal circuitry (retina → TeO → motor outputs) (Del Bene et al., 2010; Grama and Engert, 2012; Barker and Baier, 2013). Such visuo-motor processing at the level of tectum (without reaching the forebrain) may be comparable to the circuitry involved in saccade in mammals (Yamamoto and Bloch, 2017). It is possible that larval and early juvenile zebrafish behaviors are largely dependent on this tectal circuitry, and the visual system involving telencephalic circuitry becomes more important at later stages.

Evolution of ascending visual pathways

Schneider (1969) has proposed the presence of "two visual systems" terminating in the mammalian cortex (Schneider, 1969). One is called the "thalamofugal" or "geniculate" pathway, in which retinal inputs reach the striate visual cortex (V1) via a thalamic nucleus (lateral geniculate nucleus in the case of mammals). The other is

called the "tectofugal" or "extra-geniculate" pathway, in which retinal inputs reach the extrastriate visual cortex via two structures, the tectum (superior colliculus in mammals) and another thalamic nucleus (pulvinar in primates and lateral posterior nucleus in other mammals like rodents). Since then, most studies in non-mammals have been interpreted based on this notion of “two visual systems” (Hall and Ebner, 1970; Karten and Hodos, 1970; Riss and Jakway, 1970; Ingle, 1973; Karten et al., 1973; Hagio et al., 2018).

However, researchers have never reached a consensus on the evolutionary history of the tectofugal pathways. The debates have often been related to unsolved homology of the target pallial areas. The main issue is which part of the pallium would correspond to the mammalian neocortex in non-mammals such as birds (Karten and Shimizu, 1989; Bruce and Neary, 1995; Striedter, 1997; Puelles et al., 2000; Butler et al., 2011; Dugas-Ford et al., 2012) and teleosts (Braford, 1995; Wullimann and Mueller, 2004; Northcutt, 2006; Yamamoto et al., 2007; Mueller et al., 2011).

Our current study does not solve the entire evolutionary scenario in vertebrates, but at least reveals that the tectofugal pathways in amniotes and in teleosts are not homologous. In tetrapods, the neurons giving rise to the pallial projections are in the thalamus, even if the pallial projection targets are different. In contrast, our data clearly indicate that majority (if not all) of the PG neurons are of mesencephalic origin. Thus, in terms of regional homology, the teleost PG is not homologous to the amniote thalamus that is of forebrain origin. There exists a possibility that some PG cells come from a forebrain territory, as suggested by previous studies (Wullimann and Rink, 2001, 2002; Ishikawa et al., 2007). Nonetheless, in addition to the developmental criteria, the cladistics analysis also reveals the lack of evolutionary continuity of the thalamo-pallial projections.

Substantial tectofugal visual pathways to the pallium are observed only in amniotes and teleosts, and not in the intermediate taxa (Figure 9). In amphibians, the major sensory relay nucleus is the dorsal thalamus, but unlike amniotes, there are very few projections to the pallium, and the majority terminates in the subpallium (ventral telencephalon) (Kicliter, 1979; Neary and Northcutt, 1983; Wilczynski and Northcutt, 1983; Butler, 1994a). Similarly, basal groups of the actinopterygians also have a poorly developed pallial connectivity, and afferent projections from the thalamic region seem to terminate in the ventral portion of the telencephalon (Albert et al., 1999; Yamamoto et al., 1999; Holmes and Northcutt, 2003). Furthermore, in *Polypterus*, visual projection to the pallium is mediated via the nucleus medianus of the posterior tuberculum (MTP; Figure 9), which is considered to be uniquely derived in this group and not homologous to any known pathways in tetrapods (Northcutt et al., 2004; Northcutt, 2009). Indeed, there are more than two ascending pathways, with a variable abundance of each pathway depending on species (Riss and Jakway, 1970; Graybiel, 1972; Benevento and Standage, 1983; Gamlin and Cohen, 1986; Albert et al., 1999; Wild and Gaede, 2016; Heap et al., 2017).

In combination, these observations strongly suggest that the teleost and amniote pathways are not homologous to one another, but have evolved independently.

Thalamocortical-like functions by midbrain neurons in teleosts?

The amniote thalamo-pallial projection (thalamocortical projection in mammals) is a intra-forebrain projection, from the dorsal diencephalon to the dorsal telencephalon. Due to the enlargement of the forebrain in mammals especially in humans, the forebrain evolution has drawn much attention for the study of sensory processing and cognitive functions.

In contrast, our data demonstrate that the PG-pallial projection in teleosts is a midbrain-forebrain projection. This shows that a non-forebrain cell population can play an equivalent role to the thalamocortical projection neurons (conveying sensory information to the pallium). We here focused on the tectofugal visual pathway because of the availability of a zebrafish transgenic line, but PG also receives inputs of other sensory modalities (auditory, lateral line, gustatory etc.) (Striedter, 1991, 1992; Yoshimoto et al., 1998; Yamamoto and Ito, 2005, 2008; Northcutt, 2006; Ito and Yamamoto, 2009). We have previously shown that the external part of the IL, another teleost-specific multi-sensory integration center (Rink and Wullimann, 1998; Ahrens and Wullimann, 2002), is also derived from the mesencephalon (Bloch et al., 2019). More studies are needed to determine the functions of PG and IL, but these data indicate that the teleost lineage have taken an evolutionary path different from amniotes, recruiting more mesencephalic structures for sensory processing.

In addition to the variation in neuronal connectivity that we reveal here, we have already demonstrated unexpected diversity of dopamine systems, despite their involvement in similar physiological/behavioral properties across vertebrate groups (Fontaine et al., 2015; Yamamoto et al., 2015, 2017; Yamamoto and Bloch, 2017). Recently, Striedter and Northcutt (2020) have also pointed out a number of examples of convergent evolution across vertebrate taxa (Striedter and Northcutt, 2020), in agreement with our hypothesis. Taking all these data into consideration, vertebrate brains have tremendously diversified across taxa during evolution, and many similarities may be due to convergent evolution than previously thought.

Materials and methods

Zebrafish Lines

For tract-tracing study, wild-type zebrafish (*Danio rerio*) with the Oregon AB genetic background of both sexes were used.

The *Tg(gSAGFF279A)* and *Tg(UAS:GFP)* transgenic lines were generated in the National Institute of Genetics (Mishima, Japan) (Asakawa and Kawakami, 2009; Kawakami et al., 2010; Lal et al., 2018), and their offspring *Tg(gSAGFF279A;UAS:GFP)*, abbreviated *Tg(279A-GFP)*, were used in this study. This zebrafish line was maintained either by incross or by crossing with AB.

The *Tg(279A-GFP)* fish line was crossed with other transgenic lines to perform cell lineage studies. They were crossed either with the *Tg(her5:ERT2CreERT2)* (Galant et al., 2016) or *Tg(Dr830:ERT2CreERT2)* (Heuzé, 2017), plus with the *Tg(βactin:lox-stop-lox-hmgb1-mCherry)* (Wang et al., 2011; Galant et al., 2016), thus obtaining the quadruple *Tg(her5:ERT2CreERT2;βactin:lox-stop-lox-hmgb1-mCherry;279A-GFP)* or *Tg(Dr830:ERT2CreERT2;βactin:lox-stop-lox-hmgb1-mCherry;279A-GFP)*.

For *in situ* hybridization (ISH) of *ert2Cre*, double transgenic lines *Tg(her5:ERT2CreERT2;βactin:lox-stop-lox-hmgb1-mCherry)* and *Tg(Dr830:ERT2CreERT2;βactin:lox-stop-lox-hmgb1-mCherry)* were used.

Fish maintenance and staging

Zebrafish used for the biocytin tract tracing were maintained at Nagoya University (Japan) in aquaria at 22-26ºC. For the rest of the experiments, zebrafish were raised in the animal facility in Neuro-PSI (Gif-sur-Yvette, France). Embryos/larvae up to 5 days post-fertilization (dpf) were maintained and staged as described (Kimmel et al., 1995). After larval stages, zebrafish were raised in a fish facility (maintained at 26-

28°C). Zebrafish at 3 mpf or older is considered as adult. In all experiments performed in this study, we randomly used both male and female.

The experimental protocols and care of laboratory animals were conducted in compliance with the official regulatory standards and approval of the French Government (reference document n°APAFIS#1286- 2015062616102603 v5), the official Japanese regulations for research on animal, and the regulations on Animal Experiments in Nagoya University.

DiI tract-tracing

To examine brain connectivity in the adult zebrafish, we placed crystals of DiI (1,1'-dilinoleyl-3,3,3',3'-tetramethylindocarbocyanine, 4-Chlorobenzenesulfonate; FAST DiI™ solid, Thermo Fisher Scientific-Molecular Probes, D7756) in the telencephalon and the optic tectum *post-mortem*. DiI is a fluorescent lipophilic tracer that diffuses along lipid membranes, allowing both anterograde and retrograde labeling of neural processes. Adult zebrafish (n = 40) were fixed with 4% paraformaldehyde (PFA) in phosphate buffer saline (PBS) overnight at 4°C.

The brains were dissected out and a small crystal was inserted in the brain using a glass pipette. The crystal was left in the brain for dye diffusion from 10 days to 2 weeks at 37°C in PBS, or PBS containing 0.05% sodium azide to avoid fungal contamination. The brains were embedded in 3% agarose, and sectioned at 80µm (in frontal and sagittal) using a vibratome (Leica VT 1000 S).

Biocytin and BDA tract-tracing

Biocytin (Sigma-Aldrich, B4261) was injected into adult zebrafish brains (n = 40), both *in vivo* and *in vitro*. For some *in vivo* injection into TeO, BDA (molecular weight 3000;

Thermo Fisher Scientific-Molecular Probes, D7135) was also used (n=3), because labeled terminals in the PGl were clearer than that with biocytin.

For *in vivo* tract-tracing, fish were anesthetized by immersing in fresh water containing 200 mg/L tricaine methanesulfonate (MS222; Sigma-Aldrich, A5040) and set in a device for physical restraint. A small amount of fresh water containing 150-200 mg/L MS222 were poured on the fish for aeration and also to maintain the anesthetic condition. Prior to injections of biocytin into the optic nerve, extraocular muscles and the optic nerve were cut, and the eyeball was excised. Crystals of biocytin were injected into the proximal stamp of the optic nerve with a minute insect pin. For injections of biocytin into TeO and Dl, a dorsal portion of the cranium was opened with forceps to expose the brain, and crystals of biocytin were inserted into the target region with a minute insect pin.

For BDA injections into TeO, the fish were aerated with fresh water containing 85 mg/L MS222 through the mouth to maintain the anesthetic condition. A dorsal portion of the cranium was opened with a dental drill (Minimo ACE; MNA Minitor Co. Ltd.) to expose the brain, and a glass microelectrode (tip diameters: 4-14 µm) filled with 1-2% BDA solution in 0.05M Tris-HCl-buffered saline (TBS; pH 7.4) was driven into TeO with a manipulator (MN-3; Narishige). BDA was injected iontophoretically with square current pulses (+5 µA, 0.5 Hz, 50% duty cycle) passed through the electrodes for 5 minutes with a stimulator (SEN-3301; Nihon Kohden). After the injection, the orbital cavity and the cranial opening was closed with a flap made of a paraffin sheet (Parafilm, Bemis Company) or a small piece of Saran Wrap; both were affixed to the cranium with an acrylic adhesive (Aron alpha, jelly type; Toagosei).

Postoperative fish were maintained in aquaria for 1-5 hours. After the survival period, the fish were deeply anesthetized with MS222 (over 200 mg/L) and perfused

through the heart with 2% paraformaldehyde and 1% glutaraldehyde in 0.1 M phosphate buffer (PB), pH 7.4. The brains were removed from the skull and post-fixed in fresh solution of the same fixative at 4ºC for 1 to 2 days.

We also injected biocytin into the TeO, PGl, and Dl *in vitro* because it was difficult to maintain postoperative fish in aquaria for hours following injections *in vivo*. A detailed *in vitro* tract-tracing method has been reported previously (Yamamoto and Ito, 2008). Fish were deeply anesthetized with MS222 (over 200 mg/L). We quickly dissected the brain from the skull and then injected crystals of biocytin into TeO, PGl, and Dl with a minute insect pin. The brain was kept in a container filled with 50 mL normal artificial cerebrospinal fluid solution for marine teleosts (126 mM NaCl, 4.0 mM KCl, 1.0 mM $MgSO_4$, 1.7 mM $CaCl_2$ mM, 26 mM $NaHCO_3$, 1.0 mM NaH_2PO_4, and 10 mM glucose; (Tsutsui et al., 2001)) at room temperature. The solution was aerated and changed every 30 minutes. After 3-4.5 hours, we fixed the brain by immersion in 2% paraformaldehyde and 1% glutaraldehyde in 0.1 M PB for 1-3 days at 4ºC.

Tissue processing following the biocytin and BDA injection

The fixed brains were cryo-protected by immersion in 0.1 M PB containing 20% sucrose at 4ºC overnight. Cryo-protected brains were embedded in 5% agarose (type IX, ultra-low gelling temperature; Sigma-Aldrich, A2576) containing 20% sucrose and frozen in n-hexane at -60ºC. Then, frontal sections were cut at a thickness of 40 µm on a cryostat and mounted on gelatin-coated glass slides. The sections were dried for one hour at room temperature and washed once with 0.05 M TBS containing 0.1% Tween 20 (TBST) and twice with TBS each for 10 minutes. To quench non-specific peroxidase activities, sections were steeped in methanol containing 0.3% H_2O_2 for 10 minutes and washed three times with TBS and once with 0.03% TBST each for 10

minutes. Sections were incubated with a solution of avidin-biotin-peroxidase complex (1:100; VECTASTAIN Elite ABC Standard Kit, Vector Laboratories, PK-6100) overnight at room temperature. After a wash with TBST and three washes with TBS each for 10 minutes, sections were incubated for one hour with 0.5% 3,3'-diaminobenzidine (Sigma-Aldrich, D5637) solution in 0.1 M PB containing 0.04% nickel ammonium sulfate and 0.01% H_2O_2. The reaction was stopped by four times washes with TBS, and the sections were counterstained with 0.05-0.1% cresyl violet, dehydrated, and coverslipped.

Tamoxifen treatment

Tamoxifen treatments were performed in quadruple transgenic fish (see above) as described previously (Galant et al., 2016; Bloch et al., 2019). 4-Hydroxytamoxifen (Sigma-Aldrich, T176) was dissolved in ethanol at a concentration of 10 mg/ml and stored at -20°C until use. The working solution was freshly prepared before the treatment, then further diluted with embryo medium (for 24 hpf, 30 hpf, and 7 dpf) or fish water (for 2-6 wpf). The animals were incubated in the tamoxifen working solution at 28°C in the dark.

Embryos at 24 hpf and 30 hpf were dechorionated with Pronase (1 mg/ml; Sigma-Aldrich, P5147) prior to the tamoxifen treatment. Embryos were placed into the six-well culture plate (Thermo Fisher Scientific) and were incubated with embryo medium containing tamoxifen. 24 hpf embryos were treated with 10 µg/ml tamoxifen for 6 hours, and 30 hpf embryos were treated with 5 µg/ml tamoxifen for 24 hours. After the incubation, the fish were washed 3 times with embryo medium, then put back to the incubator. 7 dpf larvae were treated in a large petri dish (around 100 ml embryo

medium) with 5 µg/ml tamoxifen on 2 consecutive days, with an incubation time of 4 hours each.

For juveniles (2-6 wpf), fish were placed in a beaker (100-200 ml fish water depending on the number of fish) with an air pump, and incubated with 2 µg/ml tamoxifen on 4 consecutive days. The incubation time per day was 2-4 hours, and the treatment was interrupted whenever the fish looked sick. At the end of each incubation, the fish were gently washed 3 times with fish water, placed back to a clean fish tank and fed.

The tamoxifen treatments were performed at least twice per each developmental stage (see Supplementary file 9), and each treatment contained at least 10 individuals. The tamoxifen-induced mCherry expression was systematically observed at 3 mpf. The fish were sacrificed and double-immunofluorescence anti-GFP and anti-dsRed were performed (see below).

Tissue preparations for immunofluorescence or *in situ* hybridization (ISH)

Zebrafish embryos up to 48 hpf were fixed in ice-cold 4% paraformaldehyde (PFA; Electron Microscopy Sciences) in 0.01 M PBS containing 0.1% Tween 20 (PBST) overnight at 4°C. Zebrafish older than 5 dpf were deeply anesthetized using 0.2% tricaine methanesulfonate (MS222; Sigma-Aldrich) diluted in fish water. The fish were fixed in 4% PFA in PBST overnight at 4°C, then brains were dissected out.

Samples used for ISH were dehydrated in ethanol gradient series, and kept at −20°C in methanol at least for a couple of days. They were rehydrated prior to ISH. For immunolabeling, samples were conserved in a stocking solution containing 0.5% PFA and 0.025% sodium azide. Adult brains were sectioned in a frontal plane (80 µm) with a vibratome.

For a whole-brain imaging for zebrafish younger than 2 wpf (14 dpf), a simplified clearing protocol was applied as previously described (Affaticati et al., 2018; Bloch et al., 2019). Depigmentation was applied as follows: up to 15 larvae were incubated in 10 mL of pre-incubation solution in a petri dish (0.5X saline sodium citrate buffer (SSC), 0.1% Tween20) for 1 hour at room temperature without stirring. Then samples were bleached by incubation in depigmentation solution (0.5X SSC, 5% formamide, 3% H_2O_2). Samples were left in the solution until pigments were completely degraded. Samples were then washed 3 times in PBST and left overnight in PBST.

For tissue clearing of older zebrafish brains, a passive CLARITY technique (zPACT) was performed as described in Affaticati et al. (2017) (Affaticati et al., 2017). Dissected brains were fixed in freshly prepared ice-cold methanol-free 4% PFA in PBS (pH 7.4) at 4°C overnight. Samples were then soaked in a precooled solution of hydrogel (0.01 M PBS, 0.25% VA-044 initiator, 5% dimethyl sulfoxide, 1% PFA, 4% acrylamide, and 0.0025% bis-acrylamide) at 4°C for 2 days. The hydrogel polymerization was triggered by replacing atmospheric oxygen with nitrogen in a desiccation chamber at 37°C for 3 hours. Passive tissue clearing was performed at 37°C for 5 days in the clearing solution (8% SDS, 0.2 M boric acid, pH adjusted to 8.5) under rotation in a hybridization oven. After clearing, brains were washed in PBST at room temperature with gentle shaking for 2 days. Brains were incubated in a depigmentation solution (0.5X SSC (150 mM NaCl, 15 mM sodium citrate, pH 7.2), 5% formamide, 0.5X SSC, 3% H_2O_2, 0.1% Tween 20) for 40 min under light until all remaining pigments were bleached. After washing in PBST brains were post-fixed in PFA 4% in PBS (pH 7.4) at 4°C overnight.

Immunofluorescence

Double immunolabeling for GFP (1:1000; Aves Labs, GFP-1020; RRID: AB_10000240) and dsRed (1:600, Takara Bio, 632496; RRID: AB_10013483) was performed on adult brain sections of quadruple transgenic zebrafish. Samples were incubated in primary antibodies in PBST containing 4% NGS and 0.3% Triton X-100 at 4°C overnight. Then samples were incubated with secondary antibodies conjugated to fluorophores (1:1000; Alexa Fluor® 488 and 546, Thermo Fisher Scientific-Molecular Probes) in PBST at 4°C overnight. Goat anti-chicken antibody labelled with Alexa Fluor 488 (A-11039; RRID: AB_142924) was used for anti-GFP, and goat anti-rabbit antibody labelled with Alexa Fluor 546 (A-11010; RRID: AB_143156) was used for dsRed. The same protocol was used for single-color immunofluorescence (either GFP or dsRed only) on adult and juvenile brain sections of the parent transgenic lines. In order to visualize the brain morphology, the sections were counterstained with DAPI (4′,6-diamidino-2-phenylindole dihydrochloride; 5 µg/ml, Sigma-Aldrich) at room temperature for 20 minutes.

Immunofluorescence on larval zebrafish brains *in toto* (14 dpf or earlier) was performed as described previously (Bloch et al., 2019). Briefly, after depigmentation, samples were incubated at room temperature for 5 h in a blocking solution containing NGS, 10% dimethyl sulfoxide (DMSO), 5% PBS-glycine 1 M, 0.5% Triton X-100, 0.1% deoxycholate, and 0.1% NP-40 in PBST. Samples were then incubated in staining solution (2% NGS, 20% DMSO, 0.05% sodium azide, 0.2% Triton X-100, PBST, 10 µg/ml heparin) with anti-dsRed antibody (1:600) at room temperature for 3–4 days with gentle shaking on a 3D rocker. Secondary antibody incubation was performed for 3-4 days and DiD (Thermo Fisher Scientific-Molecular Probes L7781; 1µg/ml) labeling was added from the second day to show the whole brain morphology. Finally, samples

were incubated in a fructose-based high-refractive index (RI) solution that is adjusted to 1.457 for imaging.

CLARITY-processed adult brains were incubated in blocking solution (0.01 M PBS, 0.1% Tween 20, 1% Triton X-100, 10% dimethyl sulfoxide, 10% normal goat serum, 0.05 M glycine) at 20°C for 3 hours. Subsequently samples were incubated in staining solution (0.01 M PBS, 0.1% Tween 20, 0.1% Triton X-100, 9% dimethyl sulfoxide, 2% normal goat serum, 0.05% azide) with the chicken anti-GFP antibody (1:400) for 7 days at room temperature under gentle agitation. After four washing steps in PBST, samples were incubated in staining solution with the goat anti-chicken antibody labelled with Alexa Fluor 488 (1:400) at room temperature for 7 days. Samples were washed for 2 days in PBST and mounted in a fructose-based high refractive index solution (fHRI); 70% fructose, 20% DMSO in 0.002 M PBS, 0.005% sodium azide. The refractive index of the solution was adjusted to 1.457 using a refractometer (Kruss). The clarified samples were incubated in 50% fHRI for 6 hours and further incubated in fHRI for 1 day. For imaging, samples were mounted in 1% low melting point agarose and covered with fHRI.

In situ **hybridization (ISH)**

ISH for *ert2Cre* (Dirian et al., 2014; Galant et al., 2016; Heuzé, 2017) were performed in zebrafish brains of different developmental stages, in order to verify the expression of Cre recombinase. Detailed ISH procedures have been described in our previous publications (Affaticati et al., 2015; Xavier et al., 2017).

After rehydration, the samples were permeabilized with proteinase K (1 µg/ml; Sigma-Aldrich, P6556) at 37°C for 5-10 minutes. The proteinase K reaction was stopped by incubation with 2 µg/µl glycine. After PBST washes, the samples were

incubated in hybridization buffer at 65°C for 4 hours, then hybridized with 2 ng/ml of cRNA probe in hybridization buffer at 65°C for at least 18 hours. Samples were then washed in gradient series of formamide/2X SSC mixture at 65°C: 75% formamide/25% 2X SSC, 50% formamide/50% 2X SSC, 25% formamide/75% 2X SSC, then washed in 2X SSC and finally in 0.2X SSC. After being rinsed with PBST at room temperature, the samples were incubated with anti-digoxigenin conjugated with alkaline phosphatase (1:2500; sheep anti-DIG-AP Fab fragments, Roche Diagnostics, 11093274910; RRID: AB_514497) at 4°C overnight. After PBST washes, the signal was visualized by incubation with nitroblue tetrazolium chloride (NBT) and 5-bromo-4-chloro-3-indolylphosphate (BCIP) solution (Roche Diagnostics, 11681451001) in 0.1 M Tris-HCl (pH9.5) / 0.1 M NaCl in H_2O (TN buffer).

For embryos, the entire ISH procedures were performed *in toto*. Embryos were embedded into 3% agarose and sectioned with a vibratome in a sagittal plane (40 µm), and slide mounted for imaging. For juvenile brains, probe hybridization was performed *in toto*, and the brains were sectioned with a vitratome in a frontal plane (40 µm) before incubating with anti-DIG-AP.

Each experimental condition contained at least 4 samples for juvenile brains and at least 10 samples for embryos. The experiments were repeated at least 3 times for each developmental stage of tamoxifen treatments (see Supplementary file 8), except for 8 wpf, in which we did not observe any mCherry/GFP colocalization (see Results).

Image acquisition

A Leica TCS SP8 laser scanning confocal microscope was used to image adult sections with a 25x or 40x water immersion objective. For clarified brains, the same microscope was used with a Leica HC Fluotar L 25x/1.00 IMM motCorr objective. For

all these acquisitions, fluorescence signal was detected through photomultipliers (PMTs) after sequential laser excitation of fluorophores at 405, 488, 552 nm. Steps along the Z-axis were set at 1 µm. Epifluorescence images were acquired using a Multizoom AZ100 (Nikon).

Bright-field images were acquired with upright microscopes, either BX43 or BX60 (Olympus). Acquired images were adjusted for brightness and contrast using ImageJ/FIJI software (Schindelin et al., 2012).

Quantification of mCherry positive cells in PG

The mCherry-positive cells in the adult PG were counted from confocal images using the ImageJ cell counter plugin. We used stacks of 5 µm from frontal sections containing the medio-posterior levels of PG. The total number of cells was determined with DAPI nuclear labeling, and proportion of mCherry positive cells was calculated. The cell count was performed in the brains induced at 4 different time points: 24 hpf, 48 hpf, 2 wpf, and 3 wpf, and the average from two specimens was presented as data for each time point.

3D image reconstruction of young zebrafish brains

In order to visualize the global distribution of mCherry+ cells in the brains of larval/juvenile (5, 7, 14 dpf) zebrafish, 3D reconstruction of confocal images was performed as described in Bloch et al. (2019). A whole brain imaged in confocal microscopy was reconstructed in 3D, using Imaris 8.0.1 software (Oxford Instruments) using the “3D view” visualization tool on a Dell T3610 workstation.

Selective visualization of PGl fiber projections in *Tg(279A-GFP)*

The signal of the *Tg(279A-GFP)* was selectively visualized by manual segmentation of the fiber projections in Amira (Thermo Fisher Scientific, FEI). For the classification of the staining of the specimen, we broke down the staining pattern into four categories: background, specimen background, specimen signal, and specimen auxiliary signal that contains a widely distributed population of cells outside the scope of this study. The process of manual segmentation is an iterative succession of initial freehand (Brush) segmentation and subsequent refinement with interactive thresholding tools (Magic wand, Threshold). The segmentation was initialized by a coarse manual segmentation of the pattern of interest and was refined region by region in up to seven iterations. The rather high number of manual and threshold-based segmentation iterations is due to the auxiliary signal, which is also located in close proximity to the pattern of interest. Local thresholds for the (negative) segmentation of the auxiliary signal were adapted with respect to the voxel values of the surrounding region to a lower boundary value of 150-180 (higher boundary always was 255). The resulting regions of exceptionally bright voxels were dilated in all three dimension by two pixels for removing the auxiliary signal in their entirety from the region of interest.

For the final visualization we multiplied the original grey value dataset with the binary 3D mask of the segmentation. Since in this mask the region of interest is encoded as one (1) and the background as zero (0) the multiplication of the image with its mask will result in the separation of its original grey values within the mask from the background signal because the latter is multiplied by zero. This isolated signal was visualized using the orange-yellow colormap (look-up-table, LUT) volrenRed.col with a truncated dynamic range (0-200) for better contrast and visibility of the signal of interest in a Volren-module of Amira.

For the context of the signal of interest, we visualized in parallel the entire dataset in a separate Volren-module using a grey colormap with slightly truncated dynamic range (10-255) as a means of global contrast enhancement.

Acknowledgments

The authors thank members of Kawakami's team for their contribution for generating *Tg(gSAGFF279A)* and *Tg(UAS:GFP)* zebrafish transgenic lines. Many thanks to the members of TEFOR, notably Elodie de Job, Laurie Rivière, Elodie Machado, and Isabelle Robineau for their technical help. We also thank Matthieu Simion for his help and discussion, and Catherine Pasqualini for critical reading. We also thank members of the animal facility (especially Krystel Saroul) for taking care of zebrafish. Finally, we thank members of Laure Bally-Cuif's, Jean-Stéphan Joly's, and Philippe Vernier's team, for their support including technical, administrative, and financial help.

Author contributions

SB, HH, MT, EL, JMH, IC, and KY performed experiments. The tract-tracing study was directed by NY and the other studies were directed by KY. AH created the *Tg(Dr830:ERT2CreERT2)* transgenic line, and KS and KK created and characterized the *Tg(gSAGFF279A;UAS:GFP)* transgenic line. PA performed tissue clearing and whole-brain image acquisition, and AJ performed 3D reconstruction of the images. The data was analyzed by SB, HH, MT, NY and KY. The first draft of the manuscript was written by SB, HH, NY, and KY, and a critical revision was made by JMH, and KY.

Funding

This work was supported by CNRS, Université Paris-Saclay, Agence National de la Recherche (ANR; PALL-E-NODY), and Fondation pour la Recherche Médicale en France (Equipe FRM & Fin de thèse de sciences [FDT201805005408] ; KY & SB). It was also supported by KAKENHI Grant number JP16J03625 from Japan Society for the Promotion of Science (JSPS) to HH, NIG-JOINT (2013-A15) from National Institute of Genetics and NBRP and NBRP/Genome Information upgrading program from Japan Agency for Medical Research and Development (AMED) to KK. It also has benefited from the facilities and expertise of TEFOR - Investissement d'avenir - ANR-II-INBS-0014.

Declaration of interests

The authors declare no competing interests.

References

Affaticati P, Le Mével S, Jenett A, Rivière L, Machado E, Mughal BB, Fini J-B (2018) X-FaCT: Xenopus-Fast Clearing Technique. Methods Mol Biol 1865:233–241.

Affaticati P, Simion M, De Job E, Rivière L, Hermel J, Machado E, Joly J, Jenett A (2017) zPACT: Tissue Clearing and Immunohistochemistry on Juvenile Zebrafish Brain. Bio-Protocol 7:DOI:10.21769/BioProtoc.2636.

Affaticati P, Yamamoto K, Rizzi B, Bureau C, Peyrieras N, Pasqualini C, Demarque M, Vernier P (2015) Identification of the optic recess region as a morphogenetic entity in the zebrafish forebrain. Scientific reports 5:8738.

Ahrens K, Wullimann MF (2002) Hypothalamic inferior lobe and lateral torus connections in a percomorph teleost, the red cichlid (Hemichromis lifalili). J Comp Neurol 449:43–64.

Albert JS, Yamamoto N, Yoshimoto M, Sawai N, Ito H (1999) Visual thalamotelencephalic pathways in the sturgeon Acipenser, a non-teleost actinopterygian fish. Brain Behav Evol 53:156–172.

Asakawa K, Kawakami K (2009) The Tol2-mediated Gal4-UAS method for gene and enhancer trapping in zebrafish. Methods 49:275–281.

Barker AJ, Baier H (2013) SINs and SOMs: neural microcircuits for size tuning in the zebrafish and mouse visual pathway. Front Neural Circuits 7 Available at: https://www.ncbi.nlm.nih.gov/pmc/articles/PMC3650670/ [Accessed February 1, 2019].

Benevento LA, Standage GP (1983) The organization of projections of the retinorecipient and nonretinorecipient nuclei of the pretectal complex and layers of the superior colliculus to the lateral pulvinar and medial pulvinar in the macaque monkey. J Comp Neurol 217:307–336.

Bergquist H (1932) Zur Morphologie des Zwischenhirns bei niederen Wirbeltieren. Acta Zool:57–304.

Bloch S, Thomas M, Colin I, Galant S, Machado E, Affaticati P, Jenett A, Yamamoto K (2019) Mesencephalic origin of the inferior lobe in zebrafish. BMC Biol 17:22.

Braford MR (1995) Comparative Aspects of Forebrain Organization in the Ray-Finned Fishes: Touchstones or Not? BBE 46:259–274.

Braford MR, Northcutt RG (1983) Organization of the diencephalon and pretectum of the ray-finned fishes. In: Fish neurobiology, vol 2: Higher brain areas and

functions (Davis RE, Northcutt RG, eds), pp 117–164. Ann Arbor, MI: University of Michigan Press.

Bruce LL, Neary TJ (1995) The limbic system of tetrapods: a comparative analysis of cortical and amygdalar populations. Brain Behav Evol 46:224–234.

Butler AB (1994a) The evolution of the dorsal thalamus of jawed vertebrates, including mammals: cladistic analysis and a new hypothesis. Brain Res Brain Res Rev 19:29–65.

Butler AB (1994b) The evolution of the dorsal pallium in the telencephalon of amniotes: cladistic analysis and a new hypothesis. Brain Res Brain Res Rev 19:66–101.

Butler AB, Hodos W (2005) Comparative Vertebrate Neuroanatomy: Evolution and Adaptation (Second Edition). New Jersey: John Wiley & Sons.

Butler AB, Reiner A, Karten HJ (2011) Evolution of the amniote pallium and the origins of mammalian neocortex. Ann N Y Acad Sci 1225:14–27.

Del Bene F, Wyart C, Robles E, Tran A, Looger L, Scott EK, Isacoff EY, Baier H (2010) Filtering of visual information in the tectum by an identified neural circuit. Science 330:669–673.

Dirian L, Galant S, Coolen M, Chen W, Bedu S, Houart C, Bally-Cuif L, Foucher I (2014) Spatial regionalization and heterochrony in the formation of adult pallial neural stem cells. Developmental cell 30:123–136.

Dugas-Ford J, Rowell JJ, Ragsdale CW (2012) Cell-type homologies and the origins of the neocortex. Proceedings of the National Academy of Sciences of the United States of America 109:16974–16979.

Echevarría D, Vieira C, Gimeno L, Martínez S (2003) Neuroepithelial secondary organizers and cell fate specification in the developing brain. Brain Res Brain Res Rev 43:179–191.

Figdor MC, Stern CD (1993) Segmental organization of embryonic diencephalon. Nature 363:630–634.

Fontaine R, Affaticati P, Bureau C, Colin I, Demarque M, Dufour S, Vernier P, Yamamoto K, Pasqualini C (2015) Dopaminergic Neurons Controlling Anterior Pituitary Functions: Anatomy and Ontogenesis in Zebrafish. Endocrinology 156:2934–2948.

Furlan G, Cuccioli V, Vuillemin N, Dirian L, Muntasell AJ, Coolen M, Dray N, Bedu S, Houart C, Beaurepaire E, Foucher I, Bally-Cuif L (2017) Life-Long Neurogenic Activity of Individual Neural Stem Cells and Continuous Growth Establish an Outside-In Architecture in the Teleost Pallium. Curr Biol 27:3288-3301.e3.

Galant S, Furlan G, Coolen M, Dirian L, Foucher I, Bally-Cuif L (2016) Embryonic origin and lineage hierarchies of the neural progenitor subtypes building the zebrafish adult midbrain. Dev Biol 420:120–135.

Gamlin PD, Cohen DH (1986) A second ascending visual pathway from the optic tectum to the telencephalon in the pigeon (Columba livia). J Comp Neurol 250:296–310.

Grama A, Engert F (2012) Direction selectivity in the larval zebrafish tectum is mediated by asymmetric inhibition. Front Neural Circuits 6 Available at: https://www.ncbi.nlm.nih.gov/pmc/articles/PMC3432856/ [Accessed February 1, 2019].

Graybiel AM (1972) Some extrageniculate visual pathways in the cat. Invest Ophthalmol 11:322–332.

Güntürkün O (2005) Avian and mammalian "prefrontal cortices": limited degrees of freedom in the evolution of the neural mechanisms of goal-state maintenance. Brain research bulletin 66:311–316.

Hagio H, Sato M, Yamamoto N (2018) An ascending visual pathway to the dorsal telencephalon through the optic tectum and nucleus prethalamicus in the yellowfin goby Acanthogobius flavimanus (Temminck & Schlegel, 1845). J Comp Neurol 526:1733–1746.

Hall WC, Ebner FF (1970) Thalamotelencephalic projections in the turtle (Pseudemys scripta). J Comp Neurol 140:101–122.

Hayashi S, McMahon AP (2002) Efficient recombination in diverse tissues by a tamoxifen-inducible form of Cre: a tool for temporally regulated gene activation/inactivation in the mouse. Dev Biol 244:305–318.

Heap LA, Vanwalleghem GC, Thompson AW, Favre-Bulle I, Rubinsztein-Dunlop H, Scott EK (2017) Hypothalamic Projections to the Optic Tectum in Larval Zebrafish. Front Neuroanat 11:135.

Heuzé A (2017) Processus régénératifs du cerveau moyen dorsal chez le poisson zèbre adulte. Ph.D. thesis in French: Université Paris-Saclay, https://www.theses.fr/2017SACLS508.

Holmes PH, Northcutt RG (2003) Connections of the pallial telencephalon in the Senegal bichir, Polypterus. Brain Behav Evol 61:113–147.

Ingle D (1973) Two visual systems in the frog. Science 181:1053–1055.

Ishikawa Y, Yamamoto N, Yoshimoto M, Yasuda T, Maruyama K, Kage T, Takeda H, Ito H (2007) Developmental origin of diencephalic sensory relay nuclei in teleosts. Brain Behav Evol 69:87–95.

Ito H, Yamamoto N (2009) Non-laminar cerebral cortex in teleost fishes? Biology letters 5:117–121.

Joyner AL, Liu A, Millet S (2000) Otx2, Gbx2 and Fgf8 interact to position and maintain a mid-hindbrain organizer. Curr Opin Cell Biol 12:736–741.

Karten HJ, Hodos W (1970) Telencephalic projections of the nucleus rotundus in the pigeon (Columba livia). J Comp Neurol 140:35–51.

Karten HJ, Hodos W, Nauta WJ, Revzin AM (1973) Neural connections of the "visual wulst" of the avian telencephalon. Experimental studies in the piegon (Columba livia) and owl (Speotyto cunicularia). J Comp Neurol 150:253–278.

Karten HJ, Shimizu T (1989) The origins of neocortex: connections and lamination as distinct events in evolution. J Cogn Neurosci 1:291–301.

Kawakami K, Abe G, Asada T, Asakawa K, Fukuda R, Ito A, Lal P, Mouri N, Muto A, Suster ML, Takakubo H, Urasaki A, Wada H, Yoshida M (2010) zTrap: zebrafish gene trap and enhancer trap database. BMC Dev Biol 10:105.

Kicliter E (1979) Some telencephalic connections in the frog, Rana pipiens. J Comp Neurol 185:75–86.

Kimmel CB, Ballard WW, Kimmel SR, Ullmann B, Schilling TF (1995) Stages of embryonic development of the zebrafish. Dev Dyn 203:253–310.

Lal P, Tanabe H, Suster ML, Ailani D, Kotani Y, Muto A, Itoh M, Iwasaki M, Wada H, Yaksi E, Kawakami K (2018) Identification of a neuronal population in the telencephalon essential for fear conditioning in zebrafish. BMC Biol 16:45.

Mueller T (2012) What is the Thalamus in Zebrafish? Front Neurosci 6:64.

Mueller T, Dong Z, Berberoglu MA, Guo S (2011) The dorsal pallium in zebrafish, Danio rerio (Cyprinidae, Teleostei). Brain research 1381:95–105.

Mueller T, Wullimann MF (2002) BrdU-, neuroD (nrd)- and Hu-studies reveal unusual non-ventricular neurogenesis in the postembryonic zebrafish forebrain. Mech Dev 117:123–135.

Neary TJ, Northcutt RG (1983) Nuclear organization of the bullfrog diencephalon. J Comp Neurol 213:262–278.

Northcutt RG (2006) Connections of the lateral and medial divisions of the goldfish telencephalic pallium. J Comp Neurol 494:903–943.

Northcutt RG (2008) Forebrain evolution in bony fishes. Brain Res Bull 75:191–205.

Northcutt RG (2009) Phylogeny of nucleus medianus of the posterior tubercle in rayfinned fishes. Integr Zool 4:134–152.

Northcutt RG, Plassmann W, Holmes PH, Saidel WM (2004) A pallial visual area in the telencephalon of the bony fish Polypterus. Brain Behav Evol 64:1–10.

Puelles L, Kuwana E, Puelles E, Bulfone A, Shimamura K, Keleher J, Smiga S, Rubenstein JL (2000) Pallial and subpallial derivatives in the embryonic chick and mouse telencephalon, traced by the expression of the genes Dlx-2, Emx-1, Nkx-2.1, Pax-6, and Tbr-1. J Comp Neurol 424:409–438.

Reiner A, Yamamoto K, Karten HJ (2005) Organization and evolution of the avian forebrain. Anat Rec A Discov Mol Cell Evol Biol 287:1080–1102.

Rink E, Wullimann MF (1998) Some forebrain connections of the gustatory system in the goldfish Carassius auratus visualized by separate DiI application to the hypothalamic inferior lobe and the torus lateralis. J Comp Neurol 394:152–170.

Riss W, Jakway JS (1970) A perspective on the fundamental retinal projections of vertebrates. Brain Behav Evol 3:30–35.

Schindelin J, Arganda-Carreras I, Frise E, Kaynig V, Longair M, Pietzsch T, Preibisch S, Rueden C, Saalfeld S, Schmid B, Tinevez JY, White DJ, Hartenstein V, Eliceiri K, Tomancak P, Cardona A (2012) Fiji: an open-source platform for biological-image analysis. Nature methods 9:676–682.

Schneider GE (1969) Two visual systems. Science 163:895–902.

Stern CD, Charite J, Deschamps J, Duboule D, Durston AJ, Kmita M, Nicolas JF, Palmeirim I, Smith JC, Wolpert L (2006) Head-tail patterning of the vertebrate embryo: one, two or many unresolved problems? The International journal of developmental biology 50:3–15.

Striedter G, Northcutt RG (2020) Brains Through Time: A Natural History of Vertebrates. New York: Oxford University Press.

Striedter GF (1991) Auditory, electrosensory, and mechanosensory lateral line pathways through the forebrain in channel catfishes. J Comp Neurol 312:311–331.

Striedter GF (1992) Phylogenetic changes in the connections of the lateral preglomerular nucleus in ostariophysan teleosts: a pluralistic view of brain evolution. Brain Behav Evol 39:329–357.

Striedter GF (1997) The telencephalon of tetrapods in evolution. Brain Behav Evol 49:179–213.

Tsutsui H, Yamamoto N, Ito H, Oka Y (2001) Encoding of different aspects of afferent activities by two types of cells in the corpus glomerulosum of a teleost brain. J Neurophysiol 85:1167–1177.

Vernier P, Wullimann MF (2009) Evolution of the posterior tuberculum and preglomerular nuclear complex. In: Encyclopedia of Neuroscience (Binder MD, Hirokawa N, Windhorst U, eds). Berlin, Heidelberg: Springer.

Vieira C, Pombero A, Garcia-Lopez R, Gimeno L, Echevarria D, Martinez S (2010) Molecular mechanisms controlling brain development: an overview of neuroepithelial secondary organizers. The International journal of developmental biology 54:7–20.

von Bartheld CS, Meyer DL (1987) Comparative neurology of the optic tectum in ray-finned fishes: patterns of lamination formed by retinotectal projections. Brain Res 420:277–288.

Wang Y, Rovira M, Yusuff S, Parsons MJ (2011) Genetic inducible fate mapping in larval zebrafish reveals origins of adult insulin-producing β-cells. Development 138:609–617.

Wilczynski W, Northcutt RG (1983) Connections of the bullfrog striatum: afferent organization. J Comp Neurol 214:321–332.

Wild JM, Gaede AH (2016) Second tectofugal pathway in a songbird (Taeniopygia guttata) revisited: Tectal and lateral pontine projections to the posterior thalamus, thence to the intermediate nidopallium. J Comp Neurol 524:963–985.

Wullimann MF, Mueller T (2004) Teleostean and mammalian forebrains contrasted: Evidence from genes to behavior. J Comp Neurol 475:143–162.

Wullimann MF, Puelles L, Wicht H (1999) Early postembryonic neural development in the zebrafish: a 3-D reconstruction of forebrain proliferation zones shows their relation to prosomeres. European journal of morphology 37:117–121.

Wullimann MF, Rink E (2001) Detailed immunohistology of Pax6 protein and tyrosine hydroxylase in the early zebrafish brain suggests role of Pax6 gene in development of dopaminergic diencephalic neurons. Brain Res Dev Brain Res 131:173–191.

Wullimann MF, Rink E (2002) The teleostean forebrain: a comparative and developmental view based on early proliferation, Pax6 activity and catecholaminergic organization. Brain Res Bull 57:363–370.

Wullimann MF, Umeasalugo KE (2020) Sonic hedgehog expression in zebrafish forebrain identifies the teleostean pallidal signaling center and shows

preglomerular complex and posterior tubercular dopamine cells to arise from shh cells. J Comp Neurol 528:1321–1348.

Xavier AL, Fontaine R, Bloch S, Affaticati P, Jenett A, Demarque M, Vernier P, Yamamoto K (2017) Comparative analysis of monoaminergic cerebrospinal fluid-contacting cells in Osteichthyes (bony vertebrates). J Comp Neurol 525:2265–2283.

Yamamoto K, Bloch S (2017) Overview of Brain Evolution : Lobe-Finned Fish vs. Ray-Finned Fish. In: Evolution of the Brain, Cognition, and Emotion in Vertebrates (Watanabe S, Hofman MA, Shimizu T, eds), pp 3–33. Tokyo: Springer.

Yamamoto K, Bloch S, Vernier P (2017) New perspective on the regionalization of the anterior forebrain in Osteichthyes. Dev Growth Differ 59:175–187.

Yamamoto K, Fontaine R, Pasqualini C, Vernier P (2015) Classification of Dopamine Receptor Genes in Vertebrates: Nine Subtypes in Osteichthyes. Brain Behav Evol 86:164–175.

Yamamoto N (2009) Studies on the teleost brain morphology in search of the origin of cognition. Japanese Psychological Research 51:154–167.

Yamamoto N, Ishikawa Y, Yoshimoto M, Xue H-G, Bahaxar N, Sawai N, Yang C-Y, Ozawa H, Ito H (2007) A new interpretation on the homology of the teleostean telencephalon based on hodology and a new eversion model. Brain Behav Evol 69:96–104.

Yamamoto N, Ito H (2005) Fiber connections of the anterior preglomerular nucleus in cyprinids with notes on telencephalic connections of the preglomerular complex. J Comp Neurol 491:212–233.

Yamamoto N, Ito H (2008) Visual, lateral line, and auditory ascending pathways to the dorsal telencephalic area through the rostrolateral region of the

lateral preglomerular nucleus in cyprinids. The Journal of comparative neurology 508:615–647.

Yamamoto N, Yoshimoto M, Albert JS, Sawai N, Ito H (1999) Tectal Fiber Connections in a Non-Teleost Actinopterygian Fish, the Sturgeon Acipenser. BBE 53:142–155.

Yoshimoto M, Albert JS, Sawai N, Shimizu M, Yamamoto N, Ito H (1998) Telencephalic ascending gustatory system in a cichlid fish, Oreochromis (Tilapia) niloticus. J Comp Neurol 392:209–226.

Yu Q, Huo J, Zhang Y, Liu K, Cai Y, Xiang T, Jiang Z, Zhang L (2019) Tamoxifen-induced hepatotoxicity via lipid accumulation and inflammation in zebrafish. Chemosphere 239:124705.

Figure legends

Figure 1. Tectofugal pathways in mammals, amphibians, and teleosts and their phylogenetic relationships. Schematic drawings of sagittal brain sections of mammals, amphibians, and teleosts are shown above a phylogenetic tree of bony vertebrates (Osteichthyes). Note that tetrapods (including mammals, birds, and amphibians) and teleosts belong to two different groups of *Osteichthyes*: tetrapods are sarcopterygians (lobe-finned fish) whereas teleosts are actinopterygians (ray-finned fish). The ascending visual projections to the telencephalon are shown with red arrows. Although the connectivity patterns resemble, there are differences between taxa. The relay nucleus giving rise to the telencephalic projections is the thalamus (Th) in tetrapods, while it is the preglomerular complex (PG) in teleosts. The major telencephalic target is the pallium (Pal; indicated in green) in amniotes and in teleosts, while it is the subpallium (SPa) in amphibians. Abbreviations: Cb, cerebellum; Pal, pallium; PG, preglomerular complex; SC, superior colliculus; SPa, subpallium; TeO, optic tectum; Th, thalamus. Brain orientation: r, rostral; c, caudal; d, dorsal; v, ventral.

Figure 2. GFP+ afferents in *Tg(279A-GFP)* zebrafish transgenic line. (A and B) Frontal sections of *Tg(279A-GFP)* adult brain showing the GFP+ fibers in Dl of the pallium (A), and GFP+ cell bodies in PG (PGl) (B). The levels of the frontal sections are indicated on the schematic drawing of a lateral view of the brain (upper right). (A) Abundant GFP+ fibers are found in the zebrafish Dl, which corresponds to the main visual area observed in the goldfish pallium (upper left schematic drawing from Yamamoto, 2009 (Yamamoto, 2009)). (B) A brain section at the level of PG. Higher magnification of the right side of PG is shown in the inset. Based on the nomenclature from goldfish, we define the GFP+ PG cell cluster projecting to the Dl as PGl. (C and D) Selected

visualization of the GFP+ projections from PGl to the pallium. After 3D reconstruction of the whole brain imaging of *Tg(279A-GFP)*, the GFP+ signal of the PGl cells was selectively visualized in order to follow their projections (see Methods). (C) shows the dorsal view of the brain and (D) shows the lateral view. The original movie is shown in Video 1. Abbreviations: Dl, lateral part of dorsal telencephalic area; Dm, medial part of dorsal telencephalic area; PG, preglomerular complex; PGl, lateral preglomerular nucleus; TeO, optic tectum. Brain orientation: r, rostral; c, caudal; d, dorsal; v, ventral. Scale bars = 100 µm (A and B); 500 µm (C and D).

Figure 3. Progression of GFP expression in the *Tg(279A-GFP)* brain during development. Frontal sections of 4 wpf (A and B), 8 wpf (C and D), and the adult (E and F) brains at the level of the telencephalon (A, C, and E) and PG (B, D, and F). The approximate antero-posterior level is indicated in the schematic drawing above. At 4 wpf, there is no GFP+ fibers in Dl (A) nor GFP+ cell around PG (B). The GFP+ cells become obvious at 8 wpf (D), but their fiber labeling in Dl is significantly weaker (C) in comparison to the adult (E). Abbreviations: Dl, lateral part of dorsal telencephalic area; PG, preglomerular complex; TeO, optic tectum. Scale bar = 200 µm.

Figure 4. Tract-tracing study showing connections of the lateral preglomerular nucleus (PGl). The schematic drawing indicates the injection site of each tracer and levels of the frontal sections shown on the right panels. In all the frontal sections shown in A-L, the lateral side of the brain is shown on the left. (A-F) PGl receiving the tectal inputs. (A and B) DiI retrograde labeling (magenta), showing the injection site in PGl (A; asterisk), and a retrogradely labeled neuron (B; arrow) located in a deep layer (SPV) of the optic tectum (TeO). This neuron extends its dendrites (B; arrowheads) in the

upper layer (SFGS) where retinal projections terminate. (C and D) BDA anterograde labeling (brown) showing the injection site in TeO (C; asterisk) and anterogradely labeled terminals in the ipsilateral PGl (D; arrowheads). (E) Cresyl violet staining showing the cytoarchitecture of the zebrafish PG: the lateral (PGl) and the anterior (PGa) subdivisions can be identified, based on the comparison with the goldfish PG (the nomenclature adapted from goldfish (Yamamoto and Ito, 2008)). (F) GFP+ labeling in PG of *Tg(279A-GFP)* zebrafish line (20 µm projection of confocal images; GFP in green and DAPI in grey), showing the comparable section level shown in (E). GFP+ perikarya are mostly found in PGl. Comparison with (D) shows GFP+ neuropils are found in the area where tectal inputs terminate. (G-L) PGl neurons projecting to Dl of the pallium. (G and H) Biocytin anterograde labeling (brown) showing the injection site in PGl (G; asterisk) and anterogradely labeled terminals in the ipsilateral Dl (H). The right top inset shows a higher magnification of the squared area showing numerous labeled terminals. (I) GFP+ fiber labeling in Dl of *Tg(279A-GFP)* zebrafish line, demonstrating an arborization pattern comparable to the anterograde biocytin labeling shown in (H). (J and K) Biocytin retrograde labeling (brown) showing the injection site in the Dl (J; asterisk), and retrogradely labeled neurons in the ipsilateral PGl (K) that extend apical dendrites ramified in the neuropil. (L) GFP+ perikarya labeling in PGl of *Tg(279A-GFP)* zebrafish line (arrowheads; 5 µm projection), demonstrating the identical cell localization as shown in (K). Abbreviations: Dl, lateral part of dorsal telencephalic area; PGa, anterior preglomerular nucleus; PGl, lateral preglomerular nucleus; SAC, stratum album centrale; SFGS, stratum fibrosum et griseum superficiale; SGC, stratum griseum centrale; SPV, stratum periventriculare; TeO, optic tectum. Brain orientation: r, rostral; c, caudal; d, dorsal; v, ventral. Scale bars = 50µm (A, D-G, K, and L), 20 µm (B), 200 µm (C), 100 µm (H-J).

Figure 5. Progression of the mCherry positive cells in PG of *Tg(her5:ERT2CreERT2;βactin:lox-stop-lox-hmgb1-mCherry)* zebrafish treated with tamoxifen at 24hpf. (A) *In situ* hybridization (ISH) of *ert2Cre* showing that the expression of Cre in this line is limited to the midbrain-hindbrain boundary (MHB) at 24 hpf. (B-G) Sagittal (B, D, F) and frontal (C, E, G) views of brains showing the development of PG region. The schematic drawing of the zebrafish brain shows the position of PG (indicating the level of the frontal sections shown in C, E, and G). Higher magnifications of the PG region are shown in the insets. mCherry positive cells are shown in magenta, and brain morphology (DiD fiber labeling in B and C, DAPI in D and E) is shown in grey. (B and C) 3D reconstruction from confocal images of 5-7 dpf larval brains. The arrows indicate the PG primordium. (D-G) Adult brain sections, with DAPI (D and E) and without DAPI (F and G). The embryonic/larval images (A-C) are adapted from Bloch et al. (2019). Abbreviations: Cb, cerebellum; IL, inferior lobe; MHB, midbrain-hindbrain boundary; PG, preglomerular complex; PGa, anterior preglomerular nucleus; PGl, lateral preglomerular nucleus; Tel, telencephalon; TeO, optic tectum. Brain orientation: r, rostral; c, caudal; d, dorsal; v, ventral. Scale bars = 100 µm (A-C); 30µm (E).

Figure 6. Co-localization of GFP and mCherry in the adult PGl cells of the first quadruple transgenic line *Tg(her5:ERT2CreERT2;βactin:lox-stop-lox-hmgb1-mCherry;279A-GFP)* following the tamoxifen induction at 24 hpf. (A) Schematic drawing of the adult zebrafish brain indicating the frontal plane shown in C-F containing the PGl. (B) A single plane confocal image showing a global view of the frontal section of a 3 mpf zebrafish brain. The white square indicates the PGl shown in C-F at a higher

magnification. (C-F) A confocal image (5 µm projection) showing the co-localization of GFP and mCherry in PG (arrowheads). Inset of (E) shows the double-labeled cell at a higher magnification. Abbreviations: Dl, lateral part of dorsal telencephalic area; PG, preglomerular complex; PGa, anterior preglomerular nucleus; PGl, lateral preglomerular nucleus; Tel, telencephalon; TeO, optic tectum. Brain orientation: r, rostral; c, caudal; d, dorsal; v, ventral. Scale bars = 200 µm (B); 30 µm (C); 10µm (inset of E).

Figure 7. Expression of *ert2Cre* in the *Tg(Dr830:ERT2CreERT2)* embryonic brains. (A-C) Sagittal sections of embryonic brains (rostral to the left). At 24 hpf (A), *ert2Cre* is highly expressed in the mesencephalic domain, and a weak expression is also found in the anterior part of the brain. Later, at 30 hpf (B), the *ertCre* expression becomes limited to the mesencephalon. At 48 hpf (C), the *ertCre* expression is found exclusively in the tectal area. In C, the section plane is slightly tilted showing a more dorsal view of the embryo. Abbreviations: Mes, mesencephalic area; Tel, telencephalic area. Scale bars = 100 µm.

Figure 8. Co-localization of GFP and mCherry in the adult PGl cells of the second quadruple transgenic line *Tg(Dr830:ERT2CreERT2;βactin:lox-stop-lox-hmgb1-mCherry;279A-GFP)* following the tamoxifen induction at different developmental stages. (A-G) Confocal images (5 µm projection) of frontal sections of PGl showing the co-localization of GFP and mCherry (arrowheads). The GFP/mCherry co-localization was consistently observed in the animals induced up to 6 wpf. Co-labelled cells are shown at a higher magnification in the insets in merged images. The section plane shown here is identical to that in Figure 6. Scale bar = 30 µm.

Figure 9. Phylogenetic comparison of pallial projections in bony vertebrates (Osteichthyes). Schematic drawing of representative embryonic brains of sarcopterygians (amniote and amphibian) and actinopterygians (teleost and *Polypterus*) are shown above a phylogenetic tree of the *Osteichthyes*. Afferent projections to the pallium are shown with red arrows. The thickness of the line represents relative abundance (importance) of the pallial projections in each group. In actinopterygians, cell populations giving rise to pallial projections are not derived from the thalamic region. The basal groups of sarcopterygians and actinopterygians (e.g. amphibians and *Polypterus*) have poorly developed pallial projections. Therefore, abundant pallial projections are likely to have evolved independently in amniote and teleost lineages. Abbreviations: ac, anterior commissure; Hy, hypothalamus; MTP, nucleus medianus of the posterior tuberculum; ORR, optic recess region; Pal, pallium; PG, preglomerular complex; poc, post-optic commissure; SPa, subpallium; TeO, optic tectum; Th, thalamus. Brain orientation: r, rostral; c, caudal; d, dorsal; v, ventral.

Supplementary file 1. GFP expression of the *Tg(279A-GFP)* adult brain. (A and B) Sagittal sections of the *Tg(279A-GFP)* adult brain (anterior to the left). (A) is a more lateral level showing PG and Dl, and (B) is more medial showing the PG-pallial axonal tract (arrows). (C) Schematic drawing of a sagittal section indicating the level of the frontal sections shown in (D-L). (D-L) Frontal sections of the *Tg(279A-GFP)* adult brain from anterior to posterior. The PG-pallial projection is indicated with arrows in (F), (G), and (H). Note that the GFP expression is not exclusive to the PG-pallial projection neurons, but some other structures such as the olfactory bulb (OB) and the hypothalamus (Hy) are also labeled. Abbreviations: Cb, cerebellum; Dl, lateral part of

dorsal telencephalic area; Dm, medial part of dorsal telencephalic area; IL, inferior lobe; Hy, hypothalamus; OB, olfactory bulb; ORR, optic recess region; Pal, pallium; PGl, lateral preglomerular nucleus; SPa, subpallium; TeO, optic tectum; Tg, tegmentum. Brain orientation: r, rostral; c, caudal; d, dorsal; v, ventral. Scale bars, = 200 µm.

Supplementary file 2. Construction of *Tg(gSAGFF279A)* transgenic zebrafish. (A) The structure of the gene trap construct T2KgSAGFF. (B) The integration site of T2KgSAGFF in the *Tg(gSAGFF279A)* line. The *Tg(gSAGFF279A)* fish was analyzed by southern blot, and DNA adjacent to the insertion was cloned by inverse PCR and sequenced. The integration site was mapped within an intron of the *inpp5ka* gene on the chromosome 15 (GPCz11).

Supplementary file 3. GFP expression of the *Tg(279A-GFP)* brain at 4 wpf. Frontal sections of the juvenile brain from anterior to posterior. The approximate plane level is indicated in the schematic drawing above. The PGl-Dl projection is not observable at this stage. Abbreviations: IL, inferior lobe; Hy, hypothalamus; OB, olfactory bulb; ORR, optic recess region; Tel, telencephalon; TeO, optic tectum; Tg, tegmentum. Scale bar = 200 µm.

Supplementary file 4. Retinal projections terminating in TeO. (A-D) Frontal sections of the adult TeO (lateral to the left) visualizing biocytin injection in the optic nerve. (A) The most anterior part of TeO shown with intensively labeled optic tract (ot). (B) More posterior TeO showing the biocytin-labeled nerve terminals in the upper layer of TeO. (C) and (D) show a higher magnification of the squared areas in (B), showing the

layered cytoarchitecture of the TeO. Abbreviations: ot, optic tract; SAC, stratum album centrale; SFGS, stratum fibrosum et griseum superficiale; SGC, stratum griseum centrale; SM, stratum marginale; SO, stratum opticum; SPV, stratum periventriculare; Tel, telencephalon; TeO, optic tectum. Brain orientation: r, rostral; c, caudal; d, dorsal; v, ventral. Scale bars = 200 µm.

Supplementary file 5. Development of PG. Following tamoxifen induction at 24 hpf using *Tg(her5:ERT2CreERT2;βactin:lox-stop-lox-hmgb1-mCherry)*, distribution of mCherry positive cells in PG was observed from juvenile (19 dpf; A and 5 wpf; B) to adult (C) stages. The level of the frontal sections is indicated in the schematic drawing on the top. (A and B) mCherry positive cells at the level of PG at juvenile stages. The left half of the frontal section show the distribution of mCherry (red), whereas the right half show DAPI staining (grey) to show cytoarchitecture of the brain. At 19 dpf (A), the nucleus is labeled as "PG/TLa", because they develop as a continuous structure and not easy to distinguish until around 5 wpf (B). (C) Adult brain sections comparing the mCherry expression in *Tg(her5:ERT2CreERT2;βactin:lox-stop-lox-hmgb1-mCherry)* and GFP expression in *Tg(279A-GFP)*. Abundant mCherry+ cells are found in the adult PG, overlapping the location of GFP+ pallial projection neurons. Abbreviations: Cb, cerebellum; PG, preglomerular complex; PGl, lateral preglomerular nucleus; Tel, telencephalon, TeO, optic tectum; TLa, torus lateralis. Brain orientation: r, rostral; c, caudal; d, dorsal; v, ventral. Scale bars = 200 µm.

Supplementary file 6. Proportion of mCherry positive cells during development in PG of the second quadruple transgenic line *Tg(Dr830:ERT2CreERT2;βactin:lox-stop-lox-hmgb1-mCherry;279A-GFP)*. Proportion of mCherry positive cells in relation to the total

number of DAPI labelled cells was calculated. The dark grey represents the percentage of mCherry labeling at each induction time point, and the entire bar represents cumulative percentage including the earlier developmental stages (light grey).

Supplementary file 7. A simplified schema of the constructs of transgenic lines and order of crossing to generate the quadruple transgenic fish used for tamoxifen treatment. Two different quadruple transgenic fish were generated using either *Tg(her5:ERT2CreERT2)* (A) or *Tg(Dr830:ERT2CreERT2)* (B). The order of crossing with *Tg(βactin:lox-stop-lox-hmgb1-mCherry)* and *Tg(279A-GFP)* (which is already double transgenic) is different due to practical reasons such as maintenance efficiency and survival rate.

Supplementary file 8. Expression of *ert2Cre* in the *Tg(Dr830:ERT2CreERT2)* juvenile brains. (A-F) Frontal sections of juvenile brains showing the telencephalic (Tel) and mesencephalic (Mes) areas. The levels of the frontal sections are indicated on the schematic drawing of a lateral view of the brain. In the 2 wpf (A and B), 3 wpf (C and D), and 5 wpf (E and F) juvenile brains, *ert2Cre* is expressed exclusively in the tectal area (B, D, and F). Abbreviations: IL, inferior lobe; Mes, mesencephalic area; Tel, telencephalic area; TeO, optic tectum. Scale bars =100 µm (A-E); 200 µm (F).

Supplementary file 9. Conditions of tamoxifen treatments**.** A summary table showing experimental conditions of tamoxifen treatments in two quadruple transgenic lines: *Tg(her5:ERT2CreERT2;βactin:lox-stop-lox-hmgb1-mCherry;279A-GFP)* and *Tg(Dr830:ERT2CreERT2;βactin:lox-stop-lox-hmgb1-mCherry;279A-GFP)*. For the

latter transgenic line, the conditions were adapted depending on the developmental stages.

Video 1. 3D reconstruction of the PG-pallial visual afferents in the brain of the *Tg(279A-GFP)* transgenic line. Confocal images of the entire zebrafish brain were reconstructed to demonstrate axonal projections in 3D. Selective visualization of GFP+ signal by manual segmentaion (shown in orange) demonstrates that axonal projections originating from the PGl neurons to the ipsilateral Dl.

Video 2. 3D reconstruction of the mCherry positive cells in the 2 wpf brain of *Tg(her5:ERT2CreERT2;βactin:lox-stop-lox-hmgb1-mCherry)* zebrafish treated with tamoxifen at 24 hpf mCherry positive cells are shown in magenta, and DiD fiber labeling is shown in grey.

Figure 1

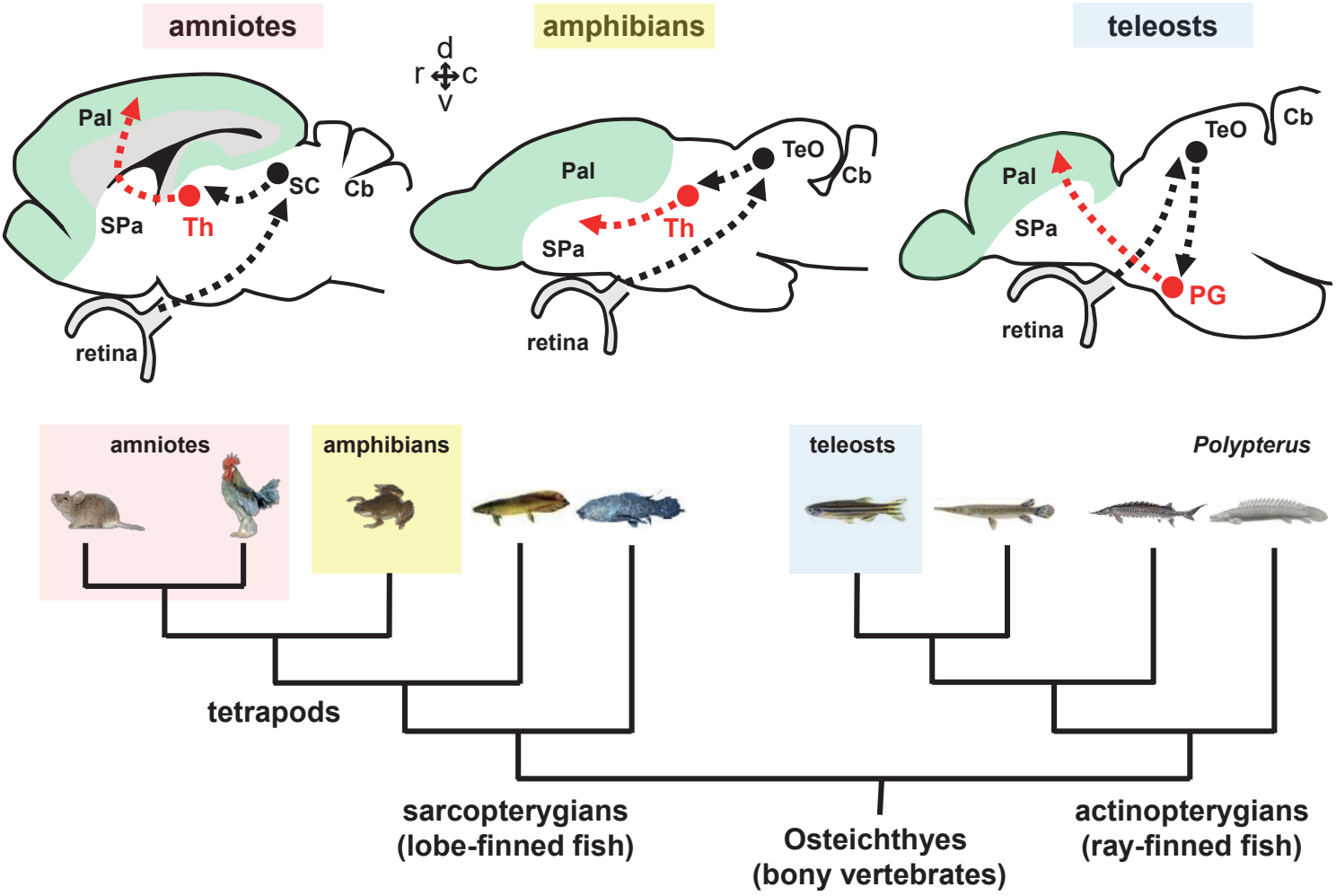

Figure 2

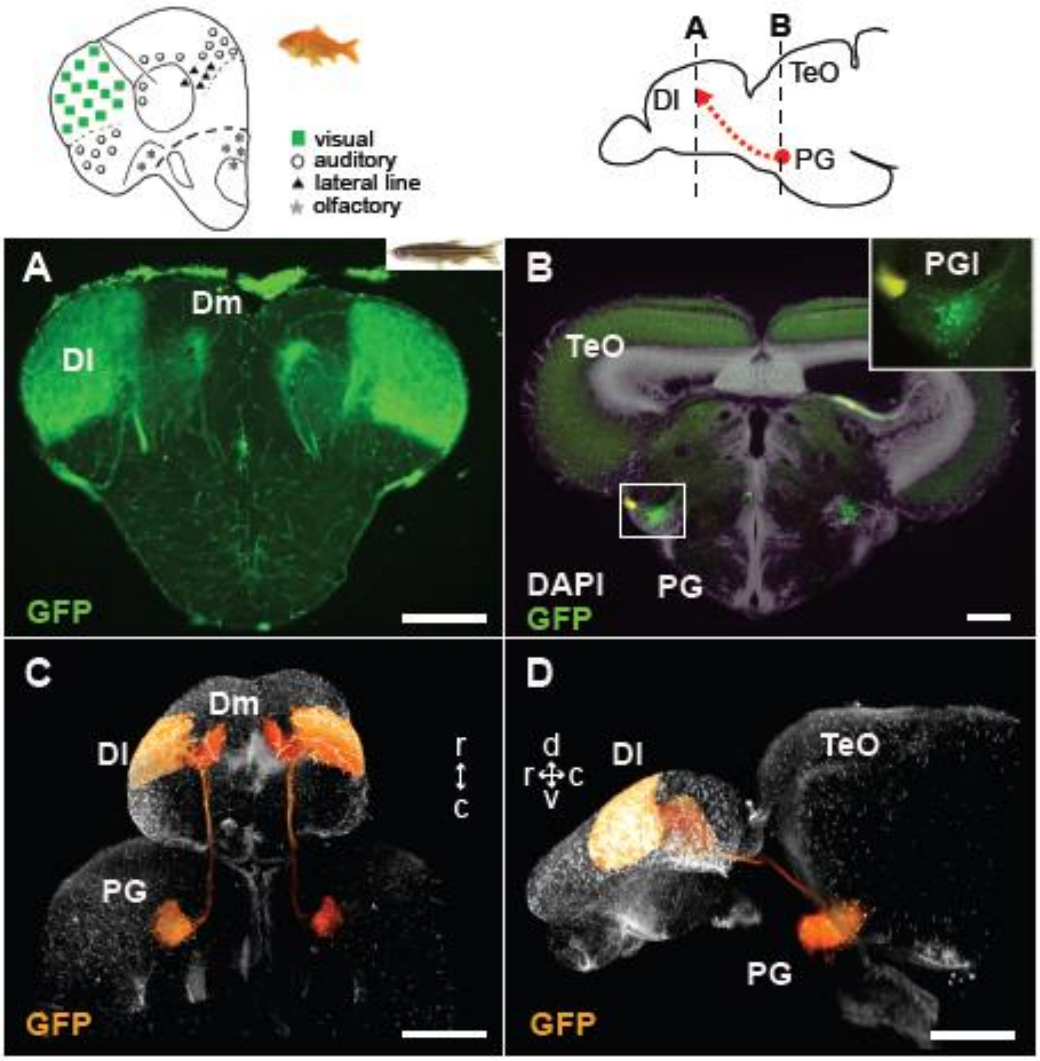

Figure 3

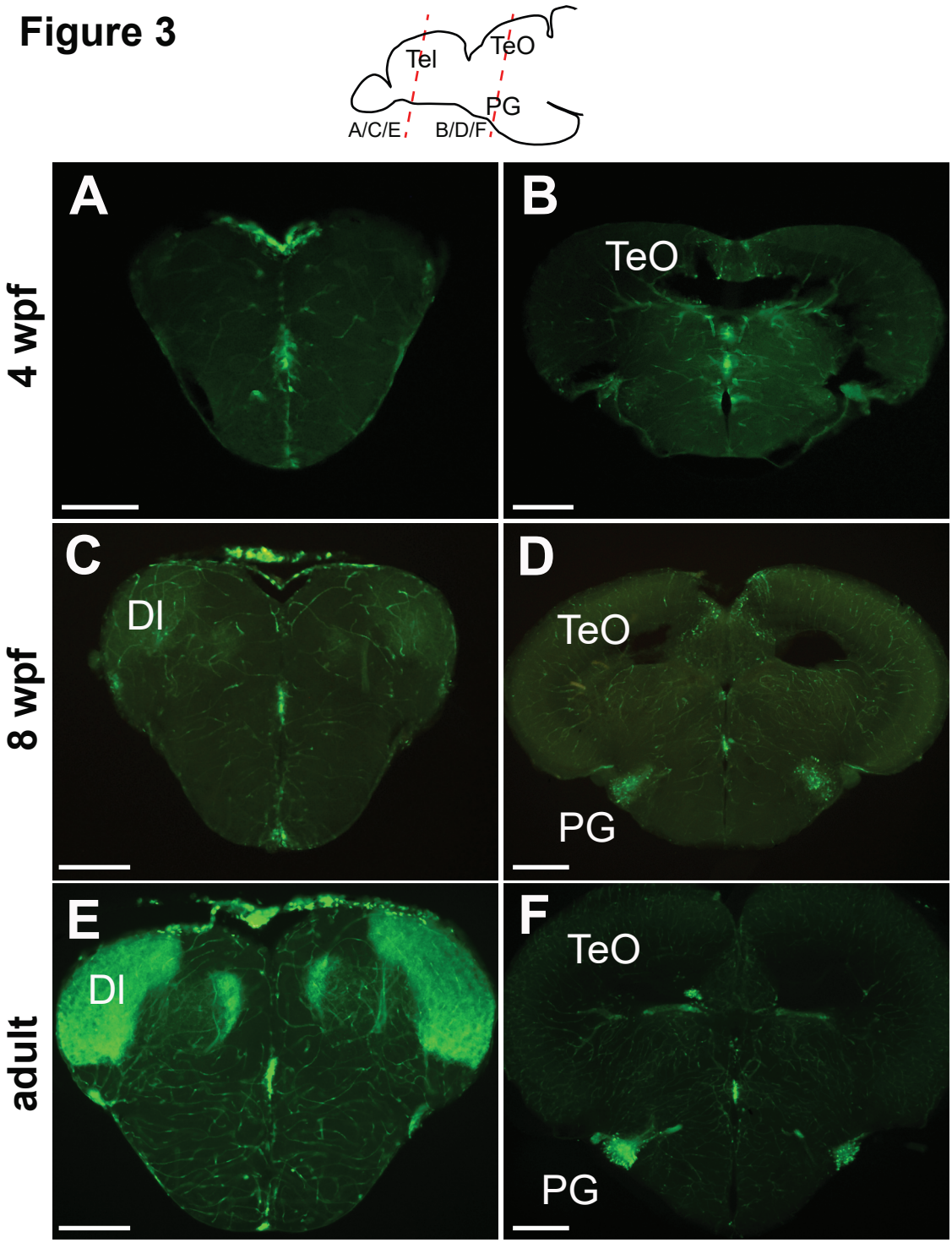

Figure 4

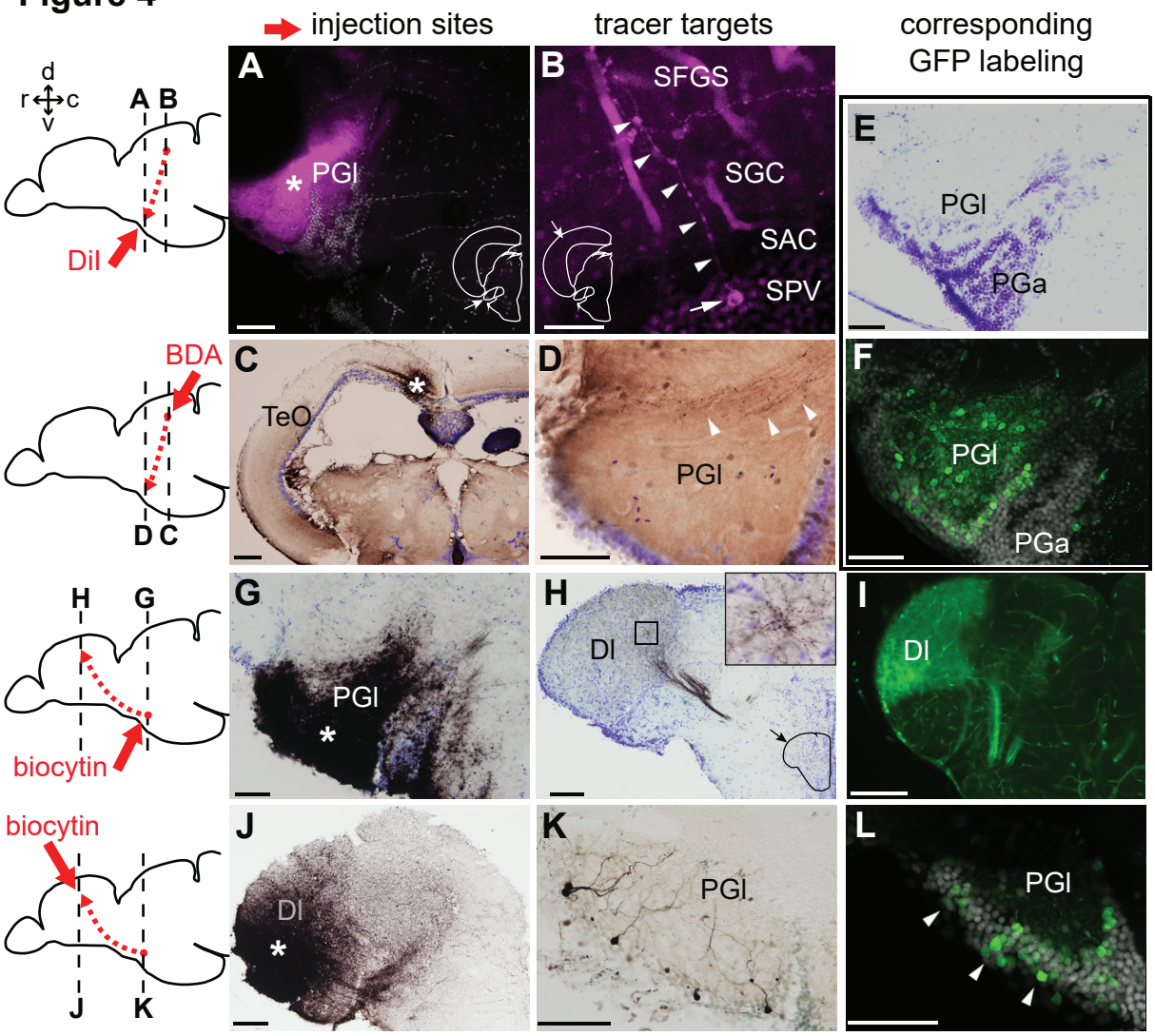

Figure 5

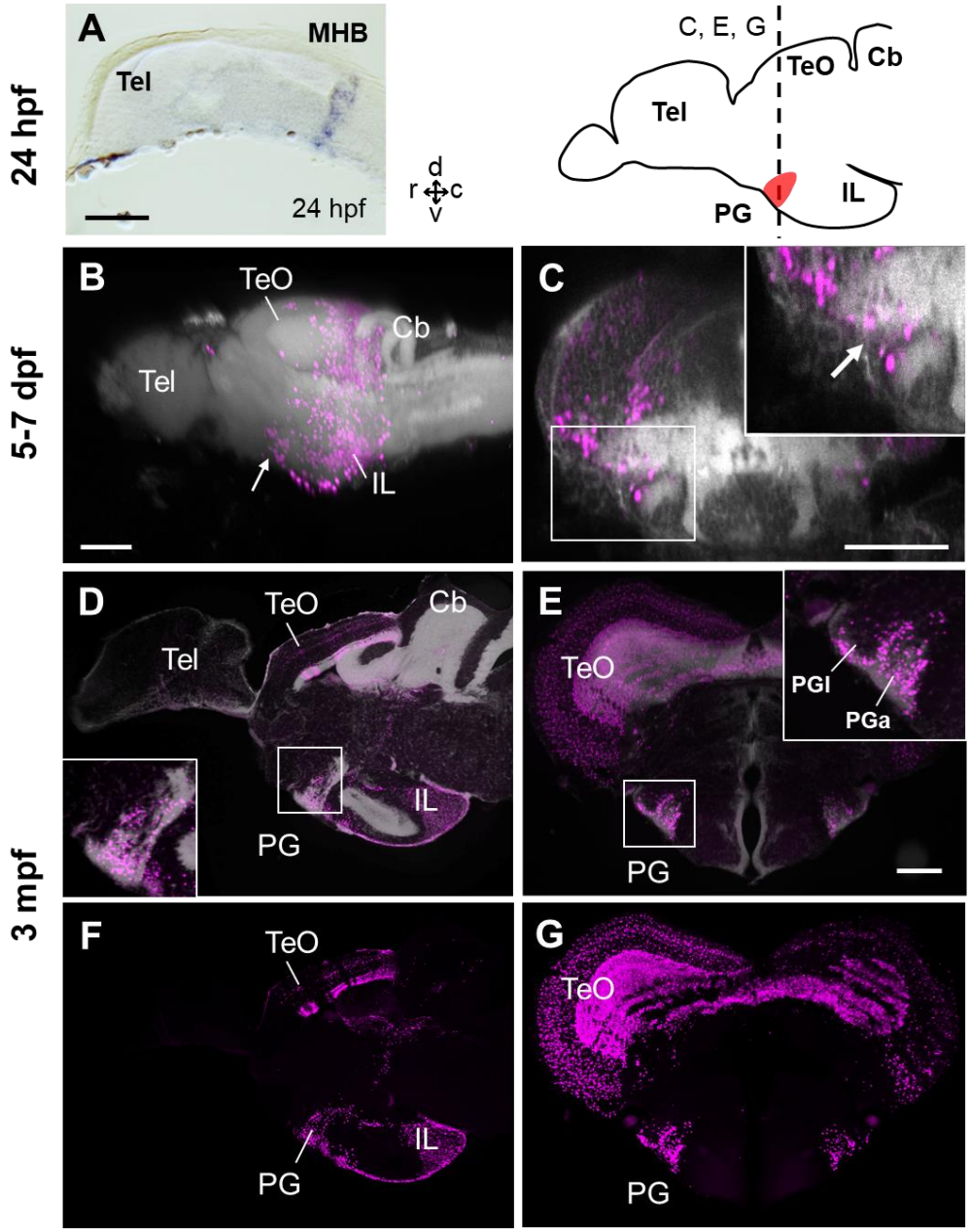

Figure 6

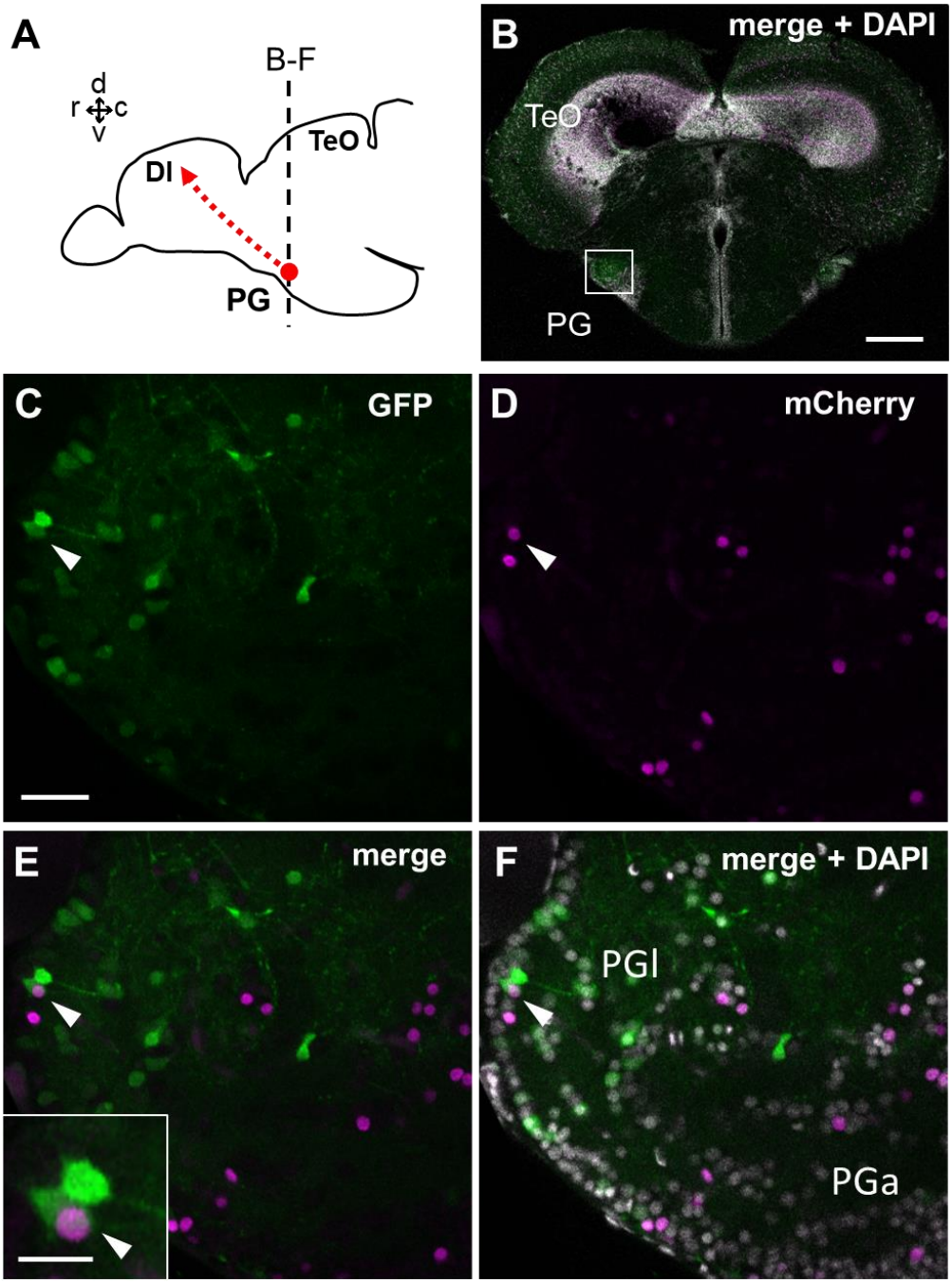

Figure 7

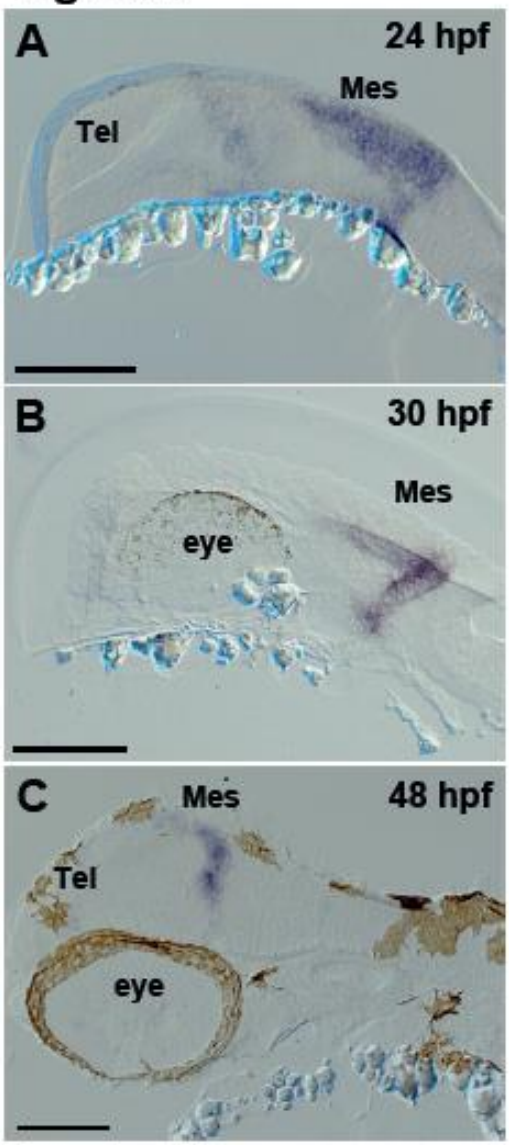

Figure 8

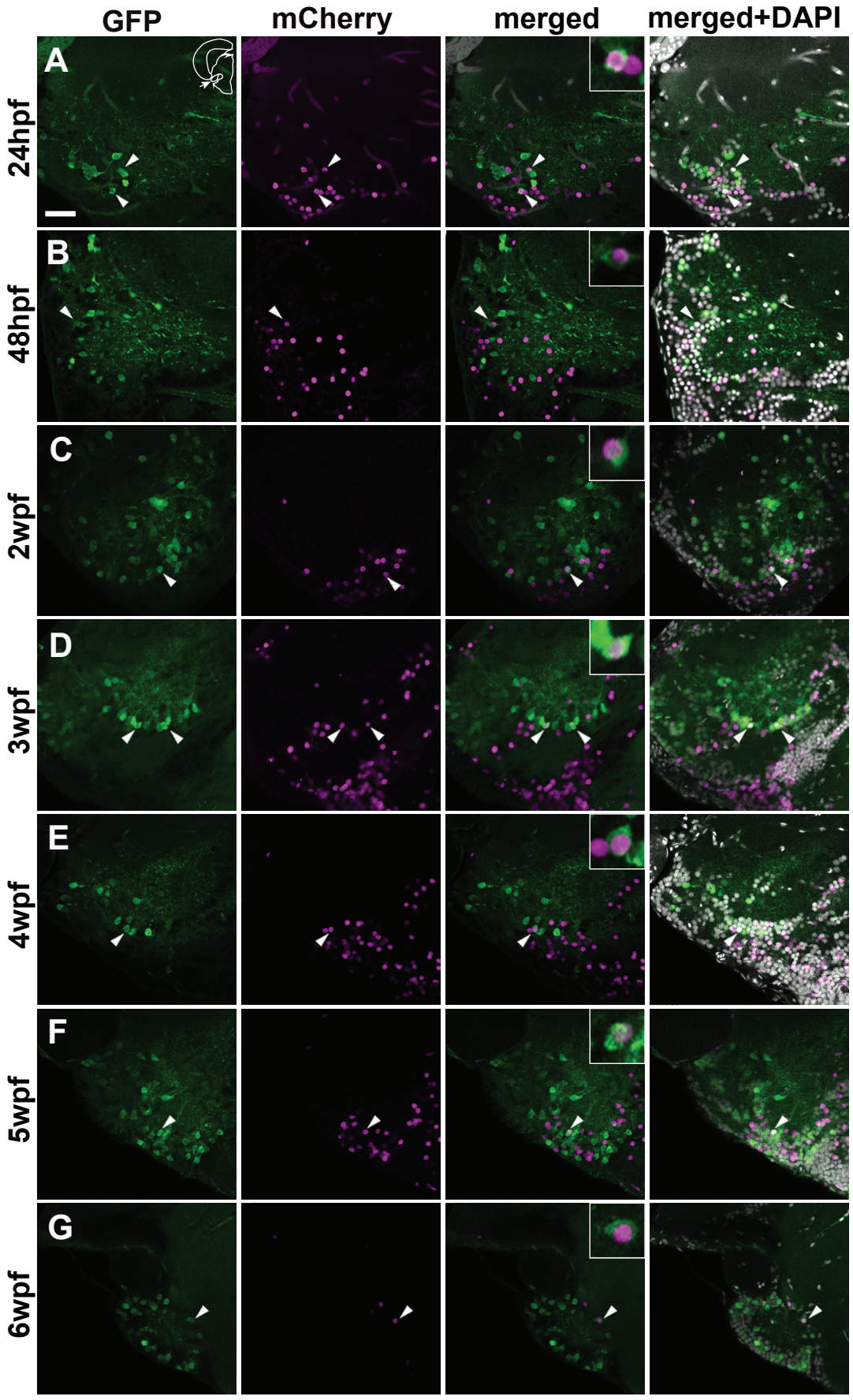

Figure 9